Remote Sensing of Environment 206 (2018) 174–188

Contents lists available at ScienceDirect

Remote Sensing of Environment

journal homepage: www.elsevier.com/locate/rse

Satellite-derived LAI products exhibit large discrepancies and can lead to substantial uncertainty in simulated carbon and water fluxes

Yibo Liu[a,b], Jingfeng Xiao[b,c,*], Weimin Ju[d], Gaolong Zhu[e], Xiaocui Wu[f], Weiliang Fan[g], Dengqiu Li[g], Yanlian Zhou[h]

[a] Jiangsu Key Laboratory of Agricultural Meteorology, School of Applied Meteorology, Nanjing University of Information Science and Technology, Nanjing 210044, China
[b] Earth Systems Research Center, Institute for the Study of Earth, Oceans, and Space, University of New Hampshire, Durham, NH 03824, USA
[c] International Center for Ecology, Meteorology, and Environment, School of Applied Meteorology, Nanjing University of Information Science and Technology, Nanjing 210044, China
[d] International Institute for Earth System Sciences, Nanjing University, Nanjing 210023, China
[e] Department of Geography, Minjiang University, Fuzhou 350108, China
[f] Center for Spatial Analysis, Department of Microbiology and Plant Biology, University of Oklahoma, OK 73019, USA
[g] Key Laboratory of Carbon Cycling in Forest Ecosystem and Carbon Sequestration of Zhejiang Province, School of Environmental & Resources Sciences, Zhejiang A & F University, Lin'an 311300, China
[h] School of Geographic and Oceanographic Sciences, Nanjing University, Nanjing 210023, China

ARTICLE INFO

Keywords:
Leaf area index
Gross primary productivity
Evapotranspiration
Uncertainty
Ecosystem model
Four-scale geometric optical model
MODIS

ABSTRACT

Understanding the terrestrial carbon and water cycles is crucial for mitigation and adaptation for climate change. Leaf area index (LAI) is a key biophysical parameter in process-based ecosystem models for simulating gross primary productivity (GPP) and evapotranspiration (ET). The uncertainty in satellite-derived LAI products and their effects on the simulation of carbon and water fluxes at regional scales remain unclear. We evaluated three satellite-derived LAI products - MODIS (MCD15), GLASS, and Four-Scale Geometric Optical Model based LAI (FSGOM) over the period 2003–2012 using fine-resolution (30 m) LAI data and field LAI measurements. GLASS had higher accuracy than FSGOM and MCD15 for forests, while FSGOM had higher accuracy than MCD15 and GLASS for grasslands. The three LAI products differed in magnitude, spatial patterns, and trends in LAI. We then examined the resulting discrepancies in simulated annual GPP and ET over China using a process-based, diagnostic terrestrial biosphere model. Mean annual total GPP for China's terrestrial ecosystems based on GLASS (6.32 $Pg\,C\,yr^{-1}$) and FSGOM (6.15 $Pg\,C\,yr^{-1}$) was 22.5% and 19.2% higher than that based on MCD15 (5.16 $Pg\,C\,yr^{-1}$), respectively. Annual GPP based on GLASS and MCD15 increased over larger fractions of China's vegetated area (15.9% and 17.3%, respectively) than that based on FSGOM (12.6%). National annual ET based on GLASS (379.9 $mm\,yr^{-1}$) and FSGOM (374.4 $mm\,yr^{-1}$) was 7.9% and 6.3% higher than that based on MCD15 (352.1 $mm\,yr^{-1}$), respectively. Simulated ET increased in larger fractions of the vegetated area for GLASS (5.7%) and MCD15 (5.8%) than for FSGOM (3.9%). Our study shows that there were large discrepancies in LAI among satellite-derived LAI products and the biases of the LAI products could lead to substantial uncertainties in simulated carbon and water fluxes.

1. Introduction

Understanding the processes of carbon and water cycles of terrestrial ecosystems is crucial for mitigation and adaptation for climate change mainly caused by increasing carbon dioxide (CO_2) concentrations in the atmosphere (IPCC, 2013). Gross primary productivity (GPP), the amount of carbon fixed by vegetation through photosynthesis, and evapotranspiration (ET), the amount of water evaporated and transpired from ecosystems, are two key components of the terrestrial carbon and water cycles. Accurate quantification of GPP and ET at regional scales is essential for assessing terrestrial carbon and water balances, wood production, agricultural productivity, and surface energy exchange. Terrestrial biosphere models have been widely used to simulate GPP and ET at various spatial scales (e.g., ecosystem, region, or the globe) (Xiao et al., 2009; Liu et al., 2016; Oleson et al., 2013).

Leaf area index (LAI), defined as one half of the total green leaf area per unit ground surface area (Chen and Black, 1992), is a key parameter in process-based ecosystem models for depicting vegetation canopy

* Corresponding author.
E-mail address: j.xiao@unh.edu (J. Xiao).

https://doi.org/10.1016/j.rse.2017.12.024
Received 11 January 2017; Received in revised form 5 December 2017; Accepted 18 December 2017
Available online 27 December 2017
0034-4257/

Table 1
Characteristics of the three LAI products (GLASS, MCD15, and FSGOM).

Products	Version	Data source	Spatial resolution	Temporal resolution	Spatial extent	Temporal extent	Reference
GLASS	V3.0	Terra/MODIS C5 reflectance	1 km	8-day	Globe	2000–2012	Xiao et al., 2014
MCD15	C5	Terra/MODIS C5 reflectance	1 km	8-day	Globe	2003–2012	Myneni et al., 2002
FSGOM	V1.0	Terra/MODIS C5 reflectance	500 m	8-day	China	2000–2014	Liu et al., 2012a

structure and simulating the exchange of mass (e.g., CO_2 and water) and energy fluxes between the land surface and the atmosphere. Process-based terrestrial biosphere models (or ecosystem models) can be generally grouped into diagnostic models and prognostic models. Diagnostic models require the prescribing of LAI using satellite-derived LAI products. Examples of diagnostic models include SiB3 (Baker et al., 2008) and BEPS (Liu et al., 1997). By contrast, prognostic models simulate LAI internally and do not rely on satellite LAI products as input, and examples include PnET-CN (Thorn et al., 2015), TEM (Xiao et al., 2009), and CLM-CN (Oleson et al., 2013).

The development of reliable gridded LAI products at regional to global scales is essential for accurate estimation of carbon and water fluxes over broad scales. These LAI products are typically based on satellite observations from different sensors, such as AVHRR (Liu et al., 2012b), MODIS (Myneni et al., 2002), and SPOT-VEGETATION (Baret et al., 2007; Deng et al., 2006). There are currently several different LAI products available at regional to global scales, including MODIS LAI (Myneni et al., 2002), GLOBMAP (Liu et al., 2012b), GIMMS (Zhu et al., 2013), GLASS LAI (Xiao et al., 2014), and FSGOM (Deng et al., 2006; Liu et al., 2012a).

Evaluating multiple LAI products can help us understand the uncertainties of these products (Morisette et al., 2006). Several previous studies have evaluated multiple LAI products (Fang et al., 2013a; Jiang et al., 2017). For example, a previous intercomparison study indicated large discrepancies among MODIS, GEOV1, GLASS, GLOBMAP, and JRC-TIP due to differences in definitions, retrieval algorithms, and input data (Fang et al., 2013a). Jiang et al. (2017) found significant discrepancies in the trends, interannual variability, and uncertainty variations among GLASS, GLOBMAP, LAI3g, and TCDR. Several studies used in-situ LAI measurements to evaluate satellite-derived LAI products and indicated significant uncertainties in and discrepancies among several existing LAI products (Cohen et al., 2003; Yang et al., 2006)

The uncertainty in the satellite-derived LAI products can lead to uncertainty in GPP and ET simulated by diagnostic ecosystem models. Input data along with model structure and model parameters are the main sources of uncertainty to model simulations (Beck, 1987). Previous studies have examined the uncertainty of model simulations resulting from input data including meteorological data (Zhao et al., 2006) and land cover (Xiao et al., 2011). Little research has assessed how the uncertainty in LAI products influence modeled carbon and water fluxes. A previous study showed that inaccurate LAI could introduce considerable uncertainties into MODIS GPP estimated from a light use efficiency model at the site level (Heinsch et al., 2006). A sensitivity analysis also revealed that simulated GPP and ET were sensitive to LAI (Ryu et al., 2011). Kala et al. (2014) examined the sensitivity of heat, moisture, and carbon fluxes of a land surface model to LAI in Australia. In addition, assimilating satellite-derived LAI into a prognostic terrestrial biosphere model improved carbon flux modeling (Demarty et al., 2007). However, the influences of the uncertainty in LAI products on regional simulation of carbon and water fluxes based on process-based ecosystem models remain unclear.

In this study, we compared and evaluated three existing satellite-derived LAI products and examined the influences of these products on annual GPP and ET of terrestrial ecosystems in China at both site and regional scales. We used a process-based diagnostic model - Boreal Ecosystem Productivity Simulator (BEPS) to simulate GPP and ET. The first objective of this study was to compare the magnitude, spatial patterns, and trends of the LAI products. The second objective was to evaluate the accuracy of the three products using Landsat-derived LAI estimates and field LAI measurements at site and regional scales. The accuracy assessment of these products (Objective 2) can explain the discrepancies among the three LAI products (Objective 1). The third objective was to assess the effects of LAI on simulated carbon and water fluxes at both site and regional scales. The discrepancies in GPP and ET among the three simulations (Objective 3) were examined based on the comparison and accuracy assessment of the LAI products (Objectives 1 and 2).

2. Data and methods

2.1. LAI data products

We used three LAI datasets derived from satellite observations from the Moderate-Resolution Imaging Spectroradiometer (MODIS): the MODIS LAI product, the Global LAnd Surface Satellite (GLASS) LAI product, and the Four-Scale Geometric Optical Model (FSGOM) based LAI product (Table 1). The MODIS LAI product (Myneni et al., 2002) is mainly retrieved based on look-up tables (LUT) simulated from three-dimensional radiative transfer models. For each biome type, vegetation clumping was accounted for at the shoot and canopy scales. The MODIS LAI product represents true LAI rather than effective LAI (Myneni et al., 2002). Several previous studies indicated that the MCD15A2 LAI product based on data from both Terra and Aqua had not only better spatial coverage and fewer data gaps (Yang et al., 2006) but also higher accuracy (Fang et al., 2012b) than the products based on data from Terra or Aqua alone. We therefore used the MODIS Terra and Aqua combined Collection 5 LAI product (MCD15A2), referred to as MCD15 hereafter, from NASA's Earth Observing System Data and Information System (EOSDIS: http://reverb.echo.nasa.gov).

We also used the GLASS LAI product, referred to as GLASS hereafter, from Beijing Normal University (http://www.bnu-datacenter.com/). GLASS was generated from MODIS surface reflectance data using a general regression neural networks (GRNNs) approach (Liang et al., 2013; Xiao et al., 2014). The effective CYCLOPES LAI was firstly converted to true LAI using clumping index (Pisek et al., 2010) and then combined with the MODIS LAI (Xiao et al., 2014). The clumping index for specific biomes was retrieved from the mean values of global clumping index values (Pisek et al., 2010) according to the MODIS land cover product: 0.73 for needleleaf forest, 0.71 for broadleaf forst, 0.77 for cropland, and 0.75 for grassland (Xiao, 2013).

The Four-Scale Geometric Optical Model based LAI, referred to as FSGOM hereafter (Liu et al., 2012a), was retrieved from MODIS reflectance using the GLOBCARBON algorithm (Deng et al., 2006). The GLOBCARBON algorithm can retrieve LAI based on the relationship between LAI and vegetation indices simulated using the four-scale geometric optical model (Chen and Leblanc, 1997). Previous studies showed that LAI inverted using this algorithm was more accurate than the MODIS LAI product (Garrigues et al., 2008; Pisek et al., 2007). Clumping index values for different vegetation types (Liu et al., 2015; Tang et al., 2007) (Table S3) were used to convert effective LAI to the true LAI. Although FSGOM is based on the same original retrieval algorithm (Deng et al., 2006) as two other LAI products: GLOBMAP (Liu et al., 2012b) and UofT (Gonsamo and Chen, 2014), these three

products were produced independently, were based on different clumping index maps, and have different time spans, spatial resolution, and spatial extent (Table S4).

These three LAI products (Table 1) have been previously used in a number of carbon and water cycling studies. MCD15 has been widely used to simulate carbon (Demarty et al., 2007; Running et al., 2004; Ryu et al., 2011) and water (Fang et al., 2016; Mu et al., 2007; Ryu et al., 2011) fluxes. GLASS has been used as model input in hydrological and ecological research (Liu et al., 2014; Sawada and Koike, 2014; Yan et al., 2016; Zhu et al., 2016). FSGOM has been used to investigate carbon and water dynamics over China's terrestrial ecosystems (Li et al., 2015; Liu et al., 2013a, 2013b; Liu et al., 2015).

2.2. Evaluation of the LAI products

The quality of the three LAI products was evaluated according to the framework "validation of global moderate-resolution LAI products" proposed by CEOS WGCV ("Committee Earth Observing Satellites' Working Group on Calibration and Validation") (Morisette et al., 2006). We used upscaled LAI maps derived from the Landsat Thematic Mapper/Enhanced Thematic Mapper (TM/ETM +) imagery (Liu et al., 2012a, 2011) to evaluate the quality of the three LAI products. A brief description about the generation and validation of these LAI maps is provided in the Supplementary material (Section 1. Landsat-based LAI maps). In this study, the upscaled 30 m-resolution LAI maps for the eight regions were aggregated to both 500 m and 1 km spatial resolutions. The resulting LAI maps, referred to as Landsat-based LAI hereafter, were used to evaluate the accuracy of the GLASS, MCD15, and FSGOM products. Only the pixels (500 m or 1 km) with percent vegetation cover ≥ 50% were considered in the evaluation.

The field plot measurements that we collected were limited to forests and grasslands, and therefore we also make use of LAI measurements from eddy covariance (EC) flux sites for multiple vegetation types. We obtained the annual maximum LAI values for 26 EC flux sites across China from the literature (Fig. 1 and Table S2). For each site, the annual maximum LAI value for each LAI product was extracted from the pixel in which the site is located. We then examined the agreement in LAI between each product and the towers.

We examined the statistical relationship of each product with reference LAI (Landsat-based and tower LAI), and used the coefficient of determination (R^2), Root Mean Square Error (RMSE), and Relative RMSE to measure the agreement between each product and the reference LAI. RRMSE is calculated as RRMSE = (RMSE / Mean) ∗ 100%, where Mean is the average reference LAI. The Taylor diagram (Taylor, 2001) was also used to measure the agreement between the Landsat-based LAI and the three LAI products across the eight regions. The Taylor diagram illustrates the following three statistical measures: correlation coefficient (R), normalized standard deviation (NSTD), and root mean square error (RMSE). The quality of each LAI product was characterized using the polar angle (R) and polar axis (NSTD) specified single point. The higher of R and the closer to 1 of the NSTD indicated better agreement between LAI products and Landsat-based LAI.

2.3. Comparison of the LAI products

We first compared the spatial patterns and magnitude of the annual mean LAI averaged over the period 2003–2012 among the three LAI products. The difference in LAI between any two of the three products was calculated to illustrate the discrepancies among the products. The distributions of LAI at the national scale were compared among vegetation types using box plots.

We also compared the trends of the annual mean LAI over the period 2003–2012 among the three LAI products on a per-pixel basis. For each pixel, the linear trend of LAI was examined by regressing LAI as a linear function of time. The significance level of 0.05 was used to examine the significance of the linear trend. We also compared the trends of the spatially-averaged LAI among the three LAI products.

2.4. GPP and ET simulations

To examine the effects of LAI on simulated carbon and water fluxes, a process-based, diagnostic ecosystem model - Boreal ecosystem production simulator (BEPS) (Liu et al., 1997) was used to simulate GPP and ET in this study. BEPS was originally stemmed from the FOREST biogeochemical model with a new temporal and spatial scaling scheme, and stratified whole canopies into sunlit and shaded leaves to calculate daily carbon fixation and water consumption (Chen et al., 1999; Liu et al., 2003). BEPS simulates GPP and ET at the daily time step. GPP of an ecosystem is the sum of photosynthetic CO_2 assimilation of canopy separately simulated by sunlit and shaded leaves. ET of an ecosystem is calculated as the sum of canopy transpiration from sunlit and shaded leaves and evaporation from soil surface and intercepted water by leaf surface. Both transpiration and evaporation are calculated using the Penman-Monteith equation. The stomatal conductance regulation was adopted from the Jarvis model (Jarvis, 1976), and stomatal conductance is regulated by environment factors including photosynthetic photon flux density, temperature, vapor pressure deficit, and soil water content (Liu et al., 2013b). The effects of elevated CO_2 on stomatal closure have not yet been taken into account in the model. Considering that the different GPP and ET trends are based on different LAI products and the same other drivers including atmospheric CO_2 concentration, the CO_2 fertilization effects do not influence the comparison of the GPP and ET trends among the different simulations. The major functions used in BEPS that are directly relevant to GPP and ET are given in the Supplementary material (2. GPP and ET algorithms in BEPS).

BEPS has been improved in many ways and has been widely used to estimate regional terrestrial carbon and water fluxes in different ecosystem types over China, North America, Europe, East Asia, and the globe (Chen et al., 2012; Liu et al., 2015; Schaefer et al., 2012; Zhang et al., 2012a). More details about the model have been fully described in previous studies (Chen et al., 1999; Ju et al., 2006; Liu et al., 2003; Liu et al., 1997).

LAI is prescribed in BEPS. Besides LAI, BEPS is driven by spatially invariant and temporally variant atmospheric CO_2 concentration data, temporally invariant soil data, and spatially and temporally explicit data on land cover and meteorology spanning the period of 2003 to 2012.

Atmospheric CO_2 concentration values were based on the annual mean CO_2 measurements at Mauna Loa Observatory, Hawaii (Keeling et al., 1976). The CO_2 time series was obtained from the National Oceanic and Atmospheric Administration's Earth System Research Laboratory (http://esrl.noaa.gov/gmd/ccgg/trends/).

We used yearly MODIS land cover datasets (MCD12Q1 V051) with the International Geosphere-Biosphere Programme (IGBP) land cover classification scheme from 2003 to 2012 (Friedl et al., 2010) to specify the land cover type for each grid cell. Soil data used here include volumetric fractions of clay, sand, and silt. These soil texture maps were developed by Shangguan et al. (2012) using the 1:1,000,000 scale soil map of China and 8595 soil profile records in the second national soil survey dataset.

The meteorological data used here include maximum and minimum air temperatures, precipitation, incoming solar radiation, and relative humidity. These gridded daily meteorological variables were interpolated from observations at 753 meteorological stations across China using the inverse distance weighted (IDW) interpolation method (Liu et al., 2015). Our previous efforts demonstrated the reliability of the gridded meteorological dataset (Liu et al., 2015).

BEPS has been parameterized for simulating the carbon and water cycling of China's terrestrial ecosystems using parameter values form the literature (Feng et al., 2007; Liu et al., 2015; Zhang et al., 2012b) and EC flux tower measurements (Liu et al., 2013a, 2013b, 2016). The values of the key biophysical and biochemical parameters used for

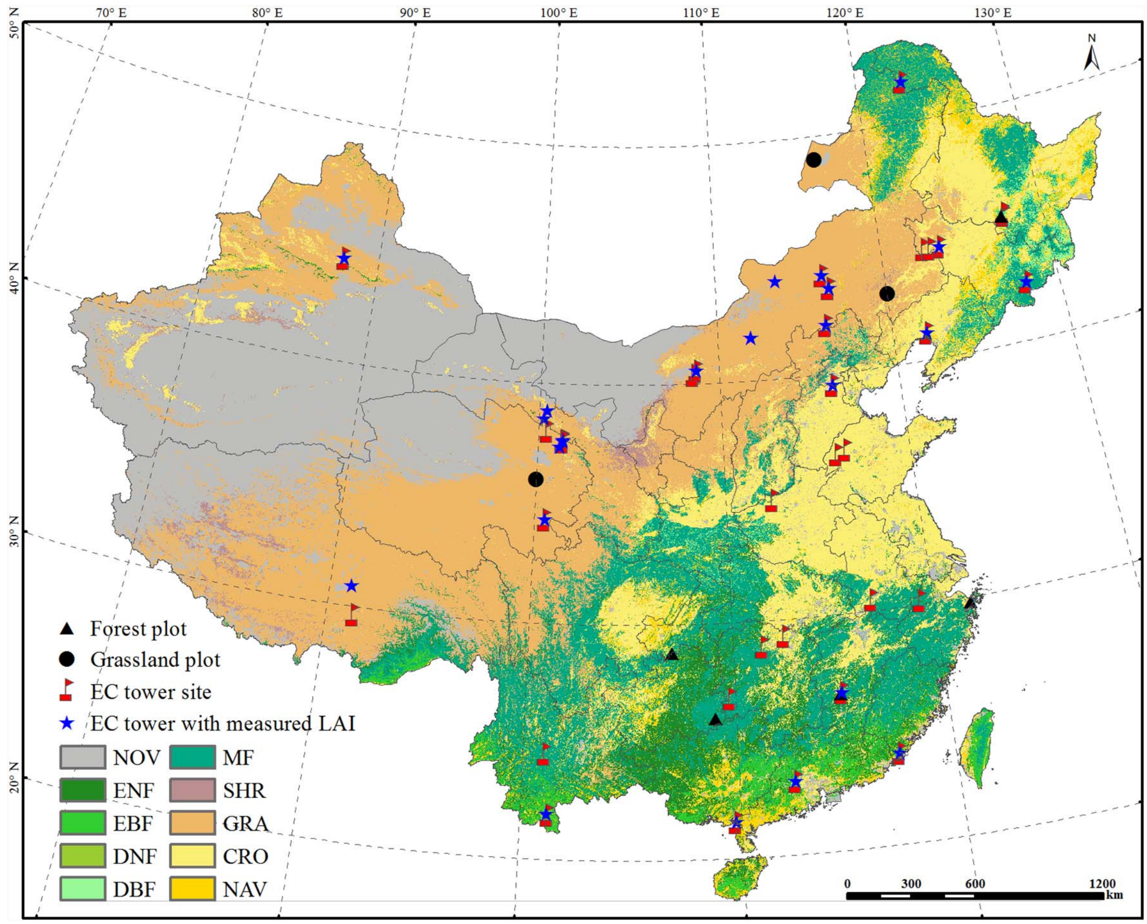

Fig. 1. Location and distribution of LAI field measurement plots and EC flux sites across China. The base map is the reclassified MODIS land-cover map. The land-cover types are as follows: evergreen needleleaf forests (ENF), evergreen broadleaf forests (EBF), deciduous needleleaf forests (DNF), deciduous broadleaf forests (DBF), mixed forests (MF), shrublands (SHR), grasslands (GRA), croplands (CRO), cropland/natural vegetation mosaic (NAV), and non-vegetation (NOV).

different vegetation types (Liu et al., 2015) are listed in Table S3.

BEPS simulated GPP and ET for each grid cell at the daily time step for the period 2003–2012. The annual GPP simulated based on the GLASS, MCD15, and FSGOM LAI products hereafter was referred to as GLASS-GPP, MCD15-GPP, and FSGOM-GPP, respectively, and the simulated annual ET was referred to as GLASS-ET, MCD15-ET and FSGOM-ET, respectively.

2.5. Comparison and evaluation of simulated GPP and ET

We obtained annual GPP data from 38 EC flux sites across China including 15 forest sites, 6 cropland sites, 14 grassland sites, and 3 wetland sites from the literature (Fig. 1 and Table S2). We also obtained annual ET from 26 EC flux sties including 9 forest sites, 12 grassland sites, 3 cropland sites, and 2 wetland sites from the literature (Fig. 1 and Table S2). The information of each site was provided in Table S2. For each site, we extracted the annual GPP and ET for each simulation for the pixel in which the site is located. We then used the tower GPP and ET to evaluate the GPP and ET simulated based on each LAI product, respectively with statistical measures: R^2, RMSE, and RRMSE.

We then compared the magnitude and spatial patterns of simulated GPP and ET based on the three LAI products, respectively. The distributions of annual GPP and ET at the national scale and for each vegetation type were compared using box plots. We examined the linear trends of GLASS-GPP, MCD15-GPP, and FSGOM-GPP on a per-pixel basis and compared the trends among the three simulations. The linear trends of the spatially-averaged GPP were also examined and compared for the three simulations. Similarly, we examined and compared the linear trends of per-pixel and spatially-averaged GLASS-ET, MCD15-ET, and FSGOM-ET.

3. Results

3.1. Comparisons of LAI products

Fig. 2 shows the spatial distributions of annual mean LAI and mutual difference for GLASS, MCD15, and FSGOM averaged over the period 2003–2012. Similarities were observed in the spatial patterns of LAI among the three products (Fig. 2a–c). For example, the mixed and evergreen forests in southern China exhibited the highest LAI, followed by the mixed forests in the Northeast, some mixed forests in the Southwest, and crop-dominated areas (e.g., North China Plains, the Southeast, Central China, and the Southwest); the vast swath of grasslands from eastern Inner Mongolia to the Qinghai-Tibet Plateau (i.e., Tibetan Plateau) exhibited low LAI. Dissimilarities were also observed in the LAI patterns. For example, the evergreen forests in the Northeast exhibited high LAI values for FSGOM and intermediate values for both GLASS and MCD15; the forests in Central China had high LAI for both GLASS and FSGOM and intermediate values for MCD15.

The magnitude of LAI also varied among the three products (Figs. 2d–f). Forested areas exhibited positive differences in LAI between FSGOM and MCD15 and between GLASS and MCD15 but negative differences between GLASS and FSGOM, indicating that FSGOM generally had the highest LAI, GLASS had intermediate values, and MCD15 had the lowest values. Croplands exhibited positive differences between GLASS and MCD15 and between GLASS and FSGOM but

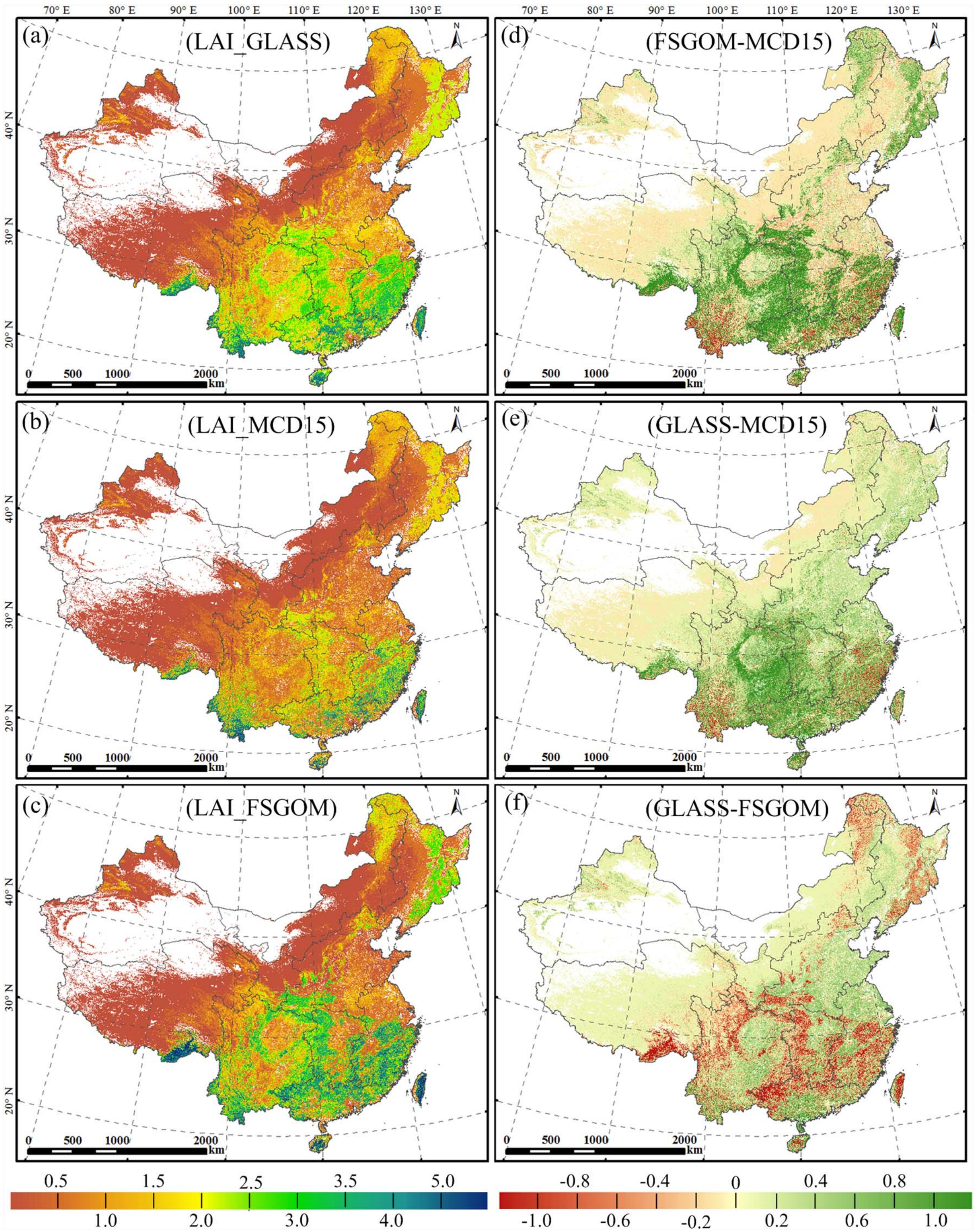

Fig. 2. Spatial patterns of annual mean LAI of the three products and the differences between each two products: (a), (b), and (c) are annual mean LAI for GLASS, MCD15, and FSGOM, respectively; (d), (e), and (f) are the differences between the FSGOM and MCD15, GLASS and MCD15, and GLASS and FSGOM, respectively. The units are $m^2\,m^{-2}$.

negative differences between FSGOM and MCD15. For croplands, GLASS generally had the highest LAI values, followed by MCD15; FSGOM had the lowest values. For grasslands, the LAI values of GLASS and MCD15 were slightly higher than those of FSGOM.

Fig. 3 shows the statistical distribution of per-pixel annual mean LAI averaged from 2003 to 2012 for each vegetation type. GLASS had slightly higher nationally-averaged LAI (0.93) than FSGOM (0.92) (one-way ANOVA, $p < 0.05$), while MCD15 exhibited much lower LAI (0.74) than the other two products (one-way ANOVA, $p < 0.05$). The LAI of evergreen needleleaf forests, deciduous broadleaf forests, and mixed forests derived from FSGOM was much higher than that of GLASS and MCD15. GLASS exhibited higher LAI than MCD15 and FSGOM in evergreen broadleaf forests, grassland, cropland and cropland/natural vegetation mosaic. The LAI estimated by MCD15 was generally lower than that by GLASS except evergreen needleleaf forests, mixed forests and deciduous broadleaf forests. For shrublands, the LAI estimated from GLASS and MCD15 were identical with each other.

Fig. 4 shows the spatial patterns of the trends in LAI on a per-pixel basis and the trends in nationally-averaged LAI values for the three products during the study period. LAI significantly increased over

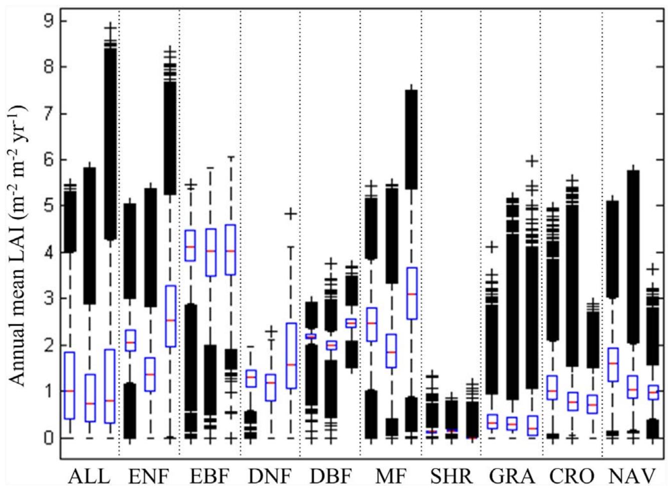

Fig. 3. Box plots of per-pixel annual mean LAI of China's terrestrial ecosystems. Each group consists of the three LAI products: GLASS, MCD15, and FSGOM (*from left to right*) for the period of 2003–2012. ALL represents the all vegetation types combined. The full name of each vegetation type is provided in the caption of Fig. 1.

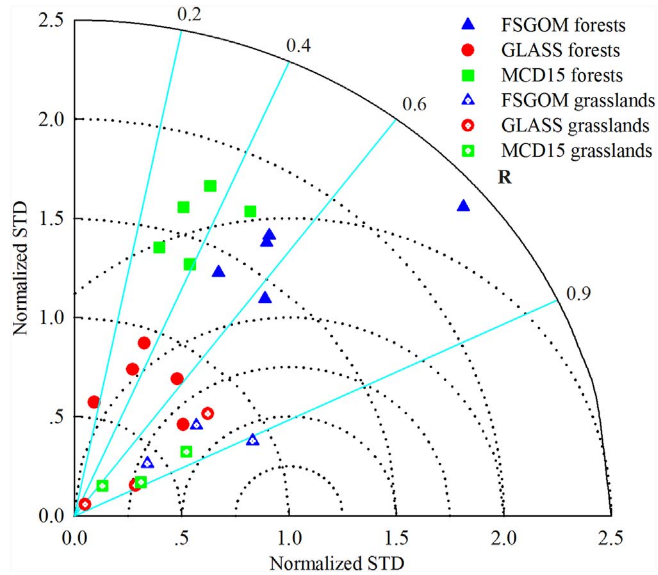

Fig. 5. Taylor diagram plot of the three different LAI products against LAI field measurement plots at eight representative regions.

14.9%, 11.7%, and 6.1% of China's vegetated area for GLASS, MCD15, and FSGOM, respectively, and significantly decreased over 7.9%, 4.3%, and 6.5% of the vegetated area for GLASS, MCD15, and FSGOM,

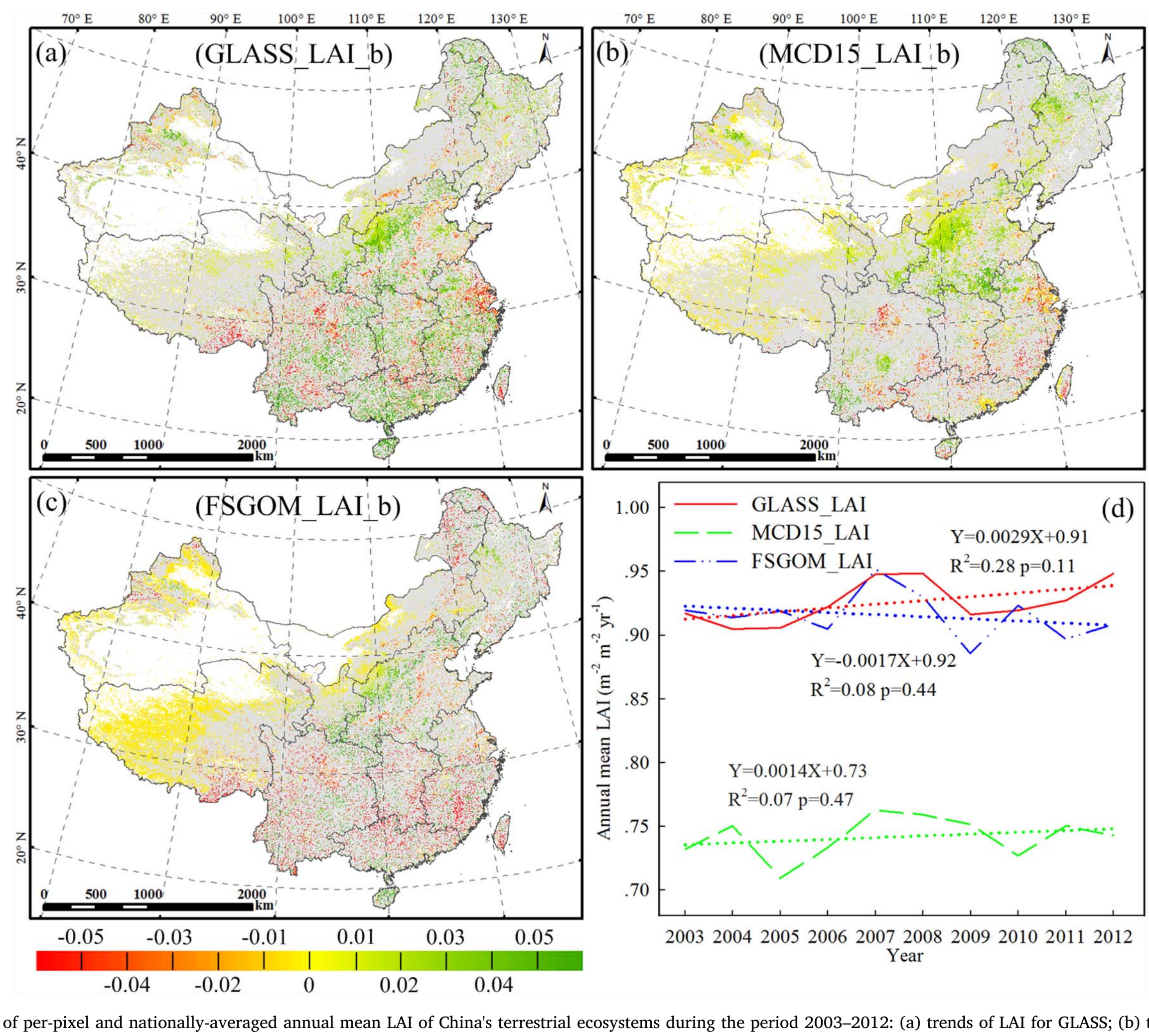

Fig. 4. Trends of per-pixel and nationally-averaged annual mean LAI of China's terrestrial ecosystems during the period 2003–2012: (a) trends of LAI for GLASS; (b) trends of LAI for MCD15, and (c) trends of LAI for FSGOM; (d) trends of nationally-averaged LAI for three products. The light gray in the (a), (b), and (c) indicates vegetated areas with insignificant trends in annual mean LAI ($p > 0.05$). The units of per-pixel LAI trends are $m^2\,m^{-2}\,yr^{-1}$.

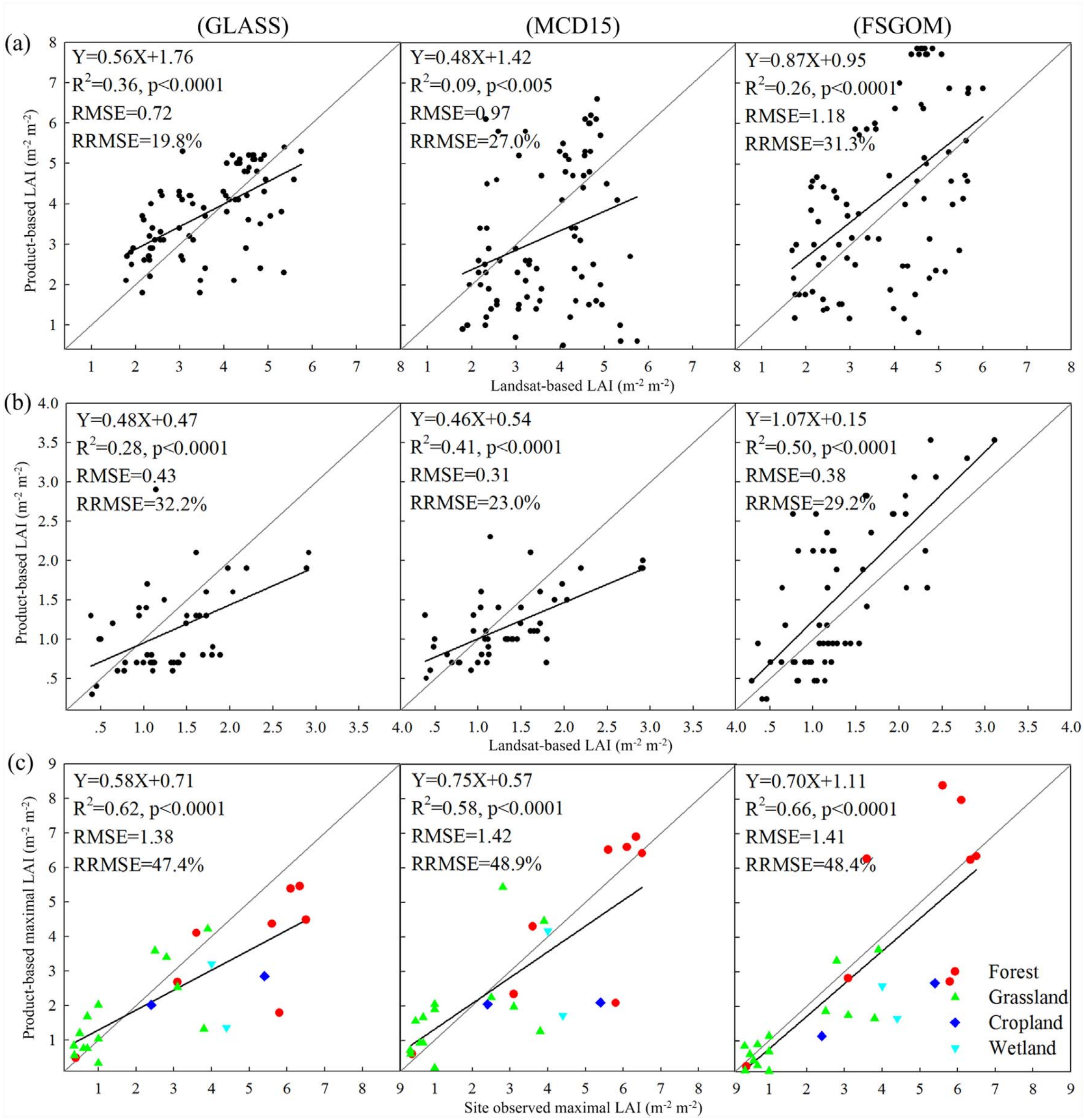

Fig. 6. Evaluation of the three LAI products: GLASS (*left column*), MCD15 (*middle column*), and FSGOM (*right column*) using field measurements in eight representative regions and EC flux sites: (a) field plots for forests; (b) field plots for grasslands; (c) EC flux sites. The units are $m^2\ m^{-2}$.

respectively. All three LAI products generally exhibited increasing trends in parts of northern China and decreasing trends in parts of southern China. Increasing trends in LAI were observed for a part of the grasslands in northern China for all three products. A part of the croplands in the Northeast and eastern China exhibited increasing trends for MCD15. Compared with MCD15 and FSGOM, GLASS showed both increasing and decreasing trends in different parts of the southern regions. The nationally-averaged LAI showed slight upward trends for GLASS and MCD15 and a slight downward trend for FSGOM during the study period (Fig. 4d), and these trends were statistically insignificant.

3.2. Evaluation of LAI products

Fig. 5 summarized the performance of three different LAI products in the eight sampling regions using the Taylor Diagram. Overall, the three LAI products performed slightly better in grasslands than in forests. For forests, FSGOM had higher R with Landsat-based LAI than GLASS and MCD 15; FSGOM had higher RMSE than GLASS and lower RMSE than MCD15; FSGOM and MCD15 had larger normalized STD or spatial variability than GLASS. For grasslands, FSGOM and GLASS had slightly higher R than MCD15; FSGOM had slightly lower RMSE than GLASS and MCD15; GLASS and MCD15 had slightly lower spatial variability than FSGOM.

Considering there were a limited number of comparison groups available while upscaling the 30 m Landsat-based LAI to coarse resolutions (500 m or 1 km), we combined Landsat-based LAI of forest and grassland together, respectively, to examine the performance of each LAI product on these two biome types. The R^2 value between the Landsat-based LAI and LAI product was 0.36, 0.09 and 0.26 for GLASS, MCD15, and FSGOM, respectively (Fig. 6a). GLASS showed lower RMSE and RRMSE (0.72; 19.8%) than MCD15 (0.97; 27.0%) and FSGOM (1.18; 31.3%) in forests. The overestimation and underestimation of GLASS occurred for forest LAI below 3.0 and above 4.5, respectively. Unlike FSGOM with systematic positive bias, MCD15 underestimated forest LAI as Landsat-based LAI values exceeded 3.0. The performances of the three LAI products in grasslands were different from their performances in forests (Fig. 6b). For grasslands, FSGOM showed the highest R^2 value (0.50) and moderate RMSE and RRMSE (0.38; 29.2%); MCD15 had higher R^2 (0.41) and lower RMSE and RRMSE (0.31; 23.0%) than GLASS. Underestimation occurred in grasslands for both

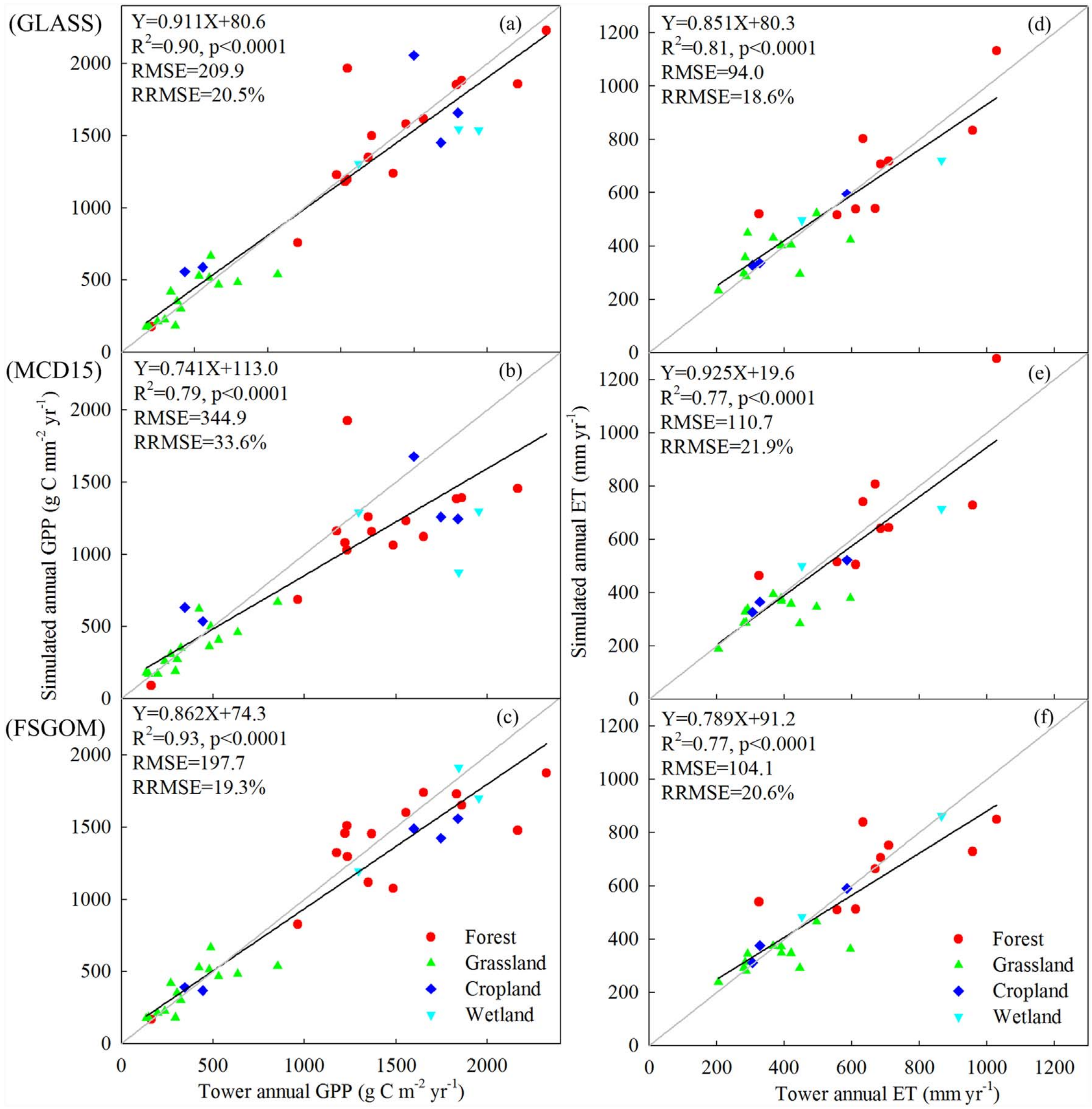

Fig. 7. Comparisons of simulated and tower annual GPP and ET. The simulated GPP (*left panel*) and ET (*right panel*) are based on GLASS (a, d), MCD15 (b, e), and FSGOM (c, f) LAI products, respectively.

MCD15 and GLASS as Landsat-based LAI exceeded 1.5.

The annual maximum LAI values derived from GLASS, MCD15, and FSGOM showed fairly good agreement with the measured LAI from EC flux sites (Fig. 6c). The R^2 value between the estimated and observed LAI varied among the three products, with FSGOM having the highest value ($R^2 = 0.66$), GLASS having the intermediate value ($R^2 = 0.62$), and MCD15 having the lowest value ($R^2 = 0.58$). MCD15 (1.41 $m^2\,m^{-2}$; 48.4%) and FSGOM (1.42 $m^2\,m^{-2}$; 48.9%) had almost identical RMSE and RRMSE, while GLASS had slightly lower RMSE and RRMSE (1.38 $m^2\,m^{-2}$; 47.4%). All these products showed different degree of underestimation. GLASS overestimated LAI for LAI < 2.0 and underestimated LAI for LAI > 2.0; MCD15 overestimated and underestimated LAI for LAI > 2.5 and LAI < 2.5, respectively; FSGOM exhibited systematic slight underestimation.

3.3. Evaluation of simulated GPP and ET based on EC flux data

The comparisons between the simulated GPP and flux tower GPP showed that the three LAI products generally led to reasonable annual GPP estimates at the site level (Fig. 7a, b, c). The fitted line for GLASS was slightly closer to the 1:1 line than that for FSGOM and much closer to the 1:1 line than that for MCD15. The R^2 values for GLASS (0.93) and FSGOM (0.90) were much higher than that for MCD15 (0.79). GLASS led to overestimation and underestimation in GPP for tower GPP ≥ and < 1000 $g\,C\,m^{-2}\,yr^{-1}$, respectively, while both MCD15 and FSGOM resulted in overestimation and underestimation for tower GPP ≥ and < 500 $g\,C\,m^{-2}\,yr^{-1}$, respectively. FSGOM-GPP and GLASS-GPP had almost identical RRMSE values (19.3% and 20.5%, respectively), which were lower than MCD15-GPP (33.6%).

The three different LAI products also generally led to reasonable estimates of annual ET (Fig. 7d, e, f). The R^2 values for GLASS (0.81), MCD15 (0.77), and FSGOM (0.77) were almost identical with each other. The fitted line for MCD15 was closer to the 1:1 line than that for GLASS or FSGOM. All three LAI simulated ET exhibited similar RRMSE values (around 20%). Both R^2 and RRMSE values for GPP were more variable than those for ET among the three LAI products, indicating that photosynthesis is likely more sensitive to vegetation LAI than is ET.

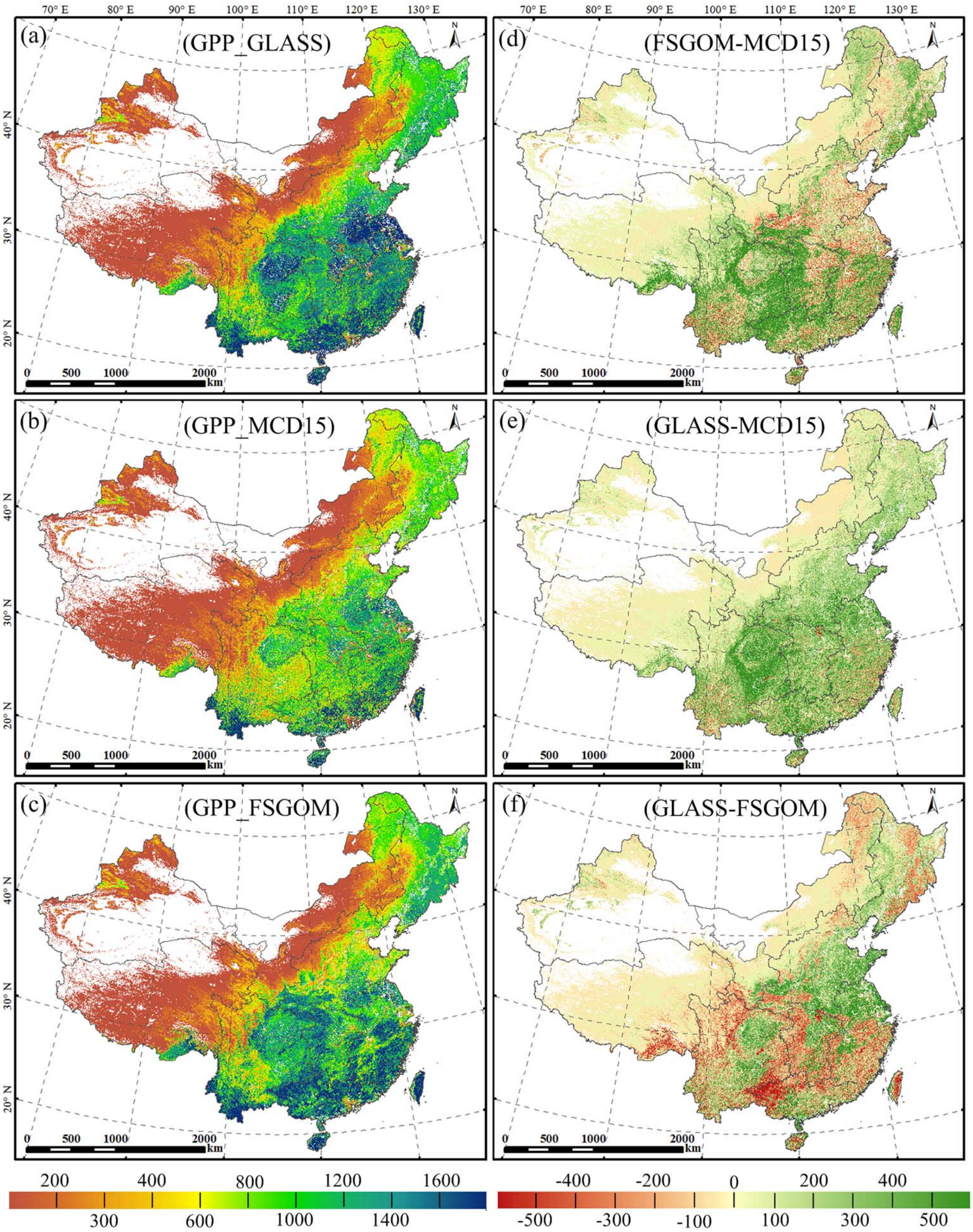

Fig. 8. Spatial patterns of annual GPP ($g\,C\,m^{-2}\,yr^{-1}$) based on the three LAI products and their differences ($g\,C\,m^{-2}\,yr^{-1}$): (a), (b), and (c) are GLASS-GPP, MCD15-GPP, and FSGOM-GPP, respectively; (d), (e), and (f) are the differences of annual GPP between FSGOM-GPP and MCD15-GPP, GLASS-GPP and MCD15-GPP, and GLASS-GPP and FSGOM-GPP, respectively.

3.4. Comparisons of simulated GPP and ET based on the three LAI products

The simulated annual GPP based on the three LAI products was generally characterized by similar spatial patterns (Fig. 8a–c): GPP increased from north to south and from west to east. These spatial patterns were mainly determined by the distribution of the land cover types and climate factors. Higher temperature and sufficient precipitation in southeastern regions provided favorable conditions for vegetation growth. These regions are dominated by forests and croplands, and these ecosystems generally had high annual GPP. The annual GPP of a large fraction of the forests and croplands in these regions was between 1400 and 1800 $g\,C\,m^{-2}\,yr^{-1}$ for GLASS and FSGOM but only between 1000 and 1400 $g\,C\,m^{-2}\,yr^{-1}$ for MCD15. The grasslands in northern and northwestern China are characterized by precipitation deficits and shorter growing season and had annual GPP ranging from 200 to 600 $g\,C\,m^{-2}\,yr^{-1}$ for all three LAI products.

Despite similar patterns, the annual GPP based on the three LAI products varied significantly in magnitude in some regions (Fig. 8d–f). GLASS-GPP was higher than MCD15-GPP for the majority of forests and croplands. The difference between the GLASS-GPP and MCD15-GPP ranged from 200 $g\,C\,m^{-2}\,yr^{-1}$ in the Northeast to 500 $g\,C\,m^{-2}\,yr^{-1}$ in the Southeast. FSGOM-GPP was higher than MCD15-GPP in forested areas but lower than MCD15-GPP in croplands. GLASS-GPP was substantially higher than FSGOM-GPP for croplands but substantially lower than FSGOM-GPP for forests.

Overall, the three LAI products led to similar spatial distribution of annual ET for China's terrestrial ecosystems: annual ET decreased from the south to the north and from the east to the west (Fig. 9a–c). These spatial patterns can be attributed to the distribution of vegetation types, precipitation, temperature and radiation that jointly regulated the transpiration and evaporation processes of different ecosystems. Despite the similar spatial patterns, the annual ET exhibited large discrepancies for some regions (Fig. 9d–f). GLASS-ET was higher than MCD15-ET in most regions covered by forests and croplands, with 20–40 $mm\,yr^{-1}$ in the Northwest and > 80 $mm\,yr^{-1}$ in southeastern regions. Large differences (> 80 $mm\,yr^{-1}$) between FSGOM-ET and MCD15-ET occurred in central, southern, and southwestern China. GLASS-ET was lower than FSGOM-ET for forests in the southern regions

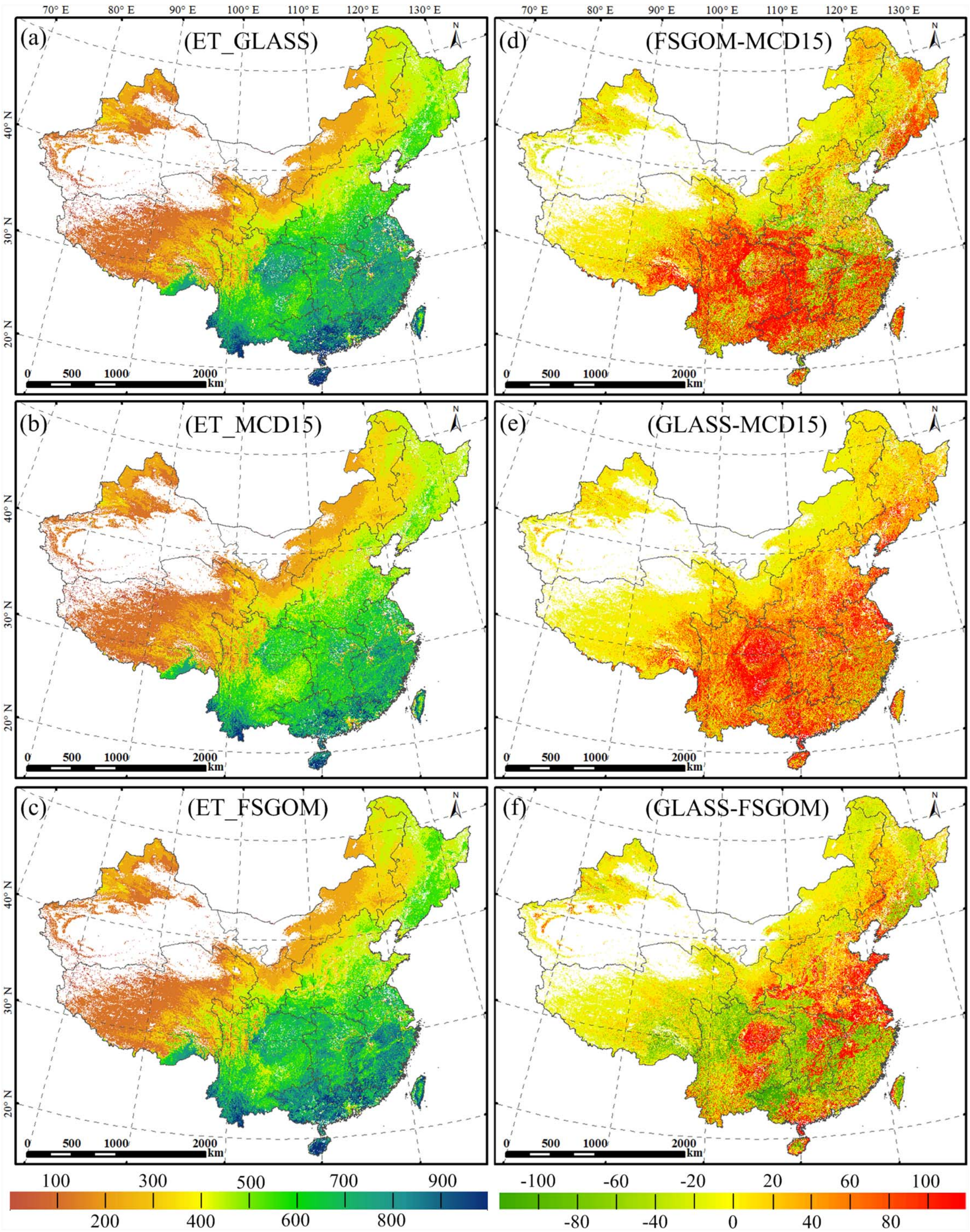

Fig. 9. Spatial patterns of annual ET (mm yr^{-1}) based on the three LAI products and their differences (mm yr^{-1}): (a), (b), and (c) are GLASS-ET, MCD15-ET, and FSGOM-ET, respectively; (d), (e), and (f) are the differences of annual ET between FSGOM-ET and MCD15-ET, GLASS-ET and MCD15-ET, and GLASS-ET and FSGOM-ET, respectively.

but higher than FSGOM-ET for croplands in southern and northern regions.

We also examined the distribution of per-pixel annual GPP and annual ET averaged from 2003 to 2012 derived from three LAI products for each vegetation type (Fig. 10). The differences in LAI (Figs. 2 and 3) led to different GPP and ET estimates. The annual mean LAI of needleleaf forests and mixed forests based on FSGOM was much higher than that of GLASS and MCD15, and consequently the simulated annual GPP and ET based on FSGOM were also higher than those based on the other two LAI products. Annual GPP and ET estimated from GLASS for croplands and cropland/natural vegetation mosaic were much higher than those from MCD15 and FSGOM. The LAI, GPP and ET based on MCD15 were generally lower than those based on GLASS with exception of grasslands. The annual mean LAI of the three LAI products and the estimated annual GPP and ET for the evergreen broadleaf forests also exhibited similar distribution patterns. However, the LAI of deciduous broadleaf forests estimated by FSGOM was higher than that of the other two LAI products, leading to higher annual GPP and ET for FSGOM than for GLASS and MCD15. For shrublands, the LAI estimated from the GLASS and MCD15 was equivalent to each other and

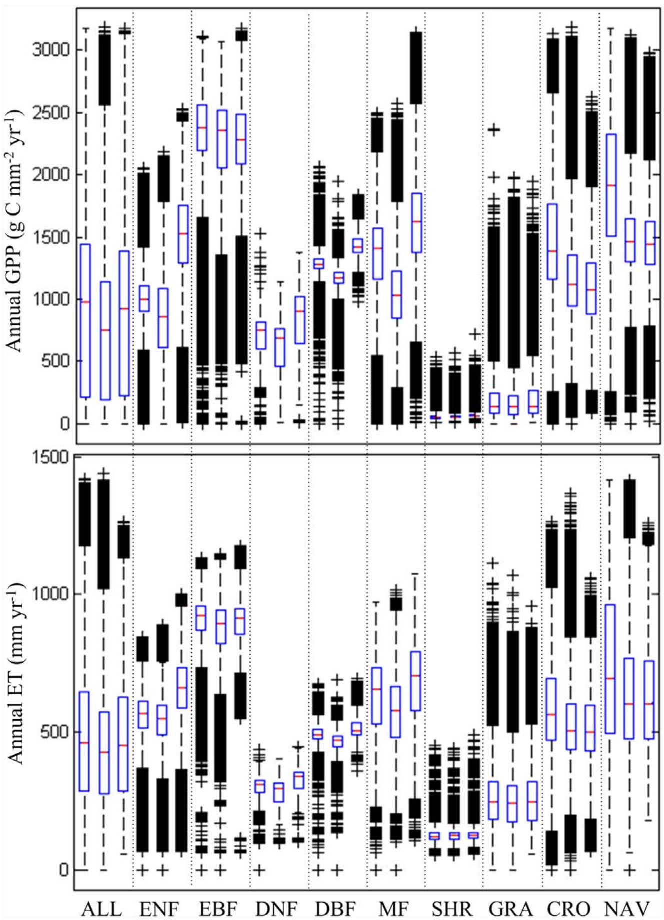

Fig. 10. Box plots of per-pixel annual GPP and annual ET of China's terrestrial ecosystems. Each group consists of GPP (a) and ET (b) for the period of 2003–2012 based on the three LAI products: GLASS, MCD15, and FSGOM (*from left to right*). ALL stands for spatially-averaged annual GPP or ET for all vegetation types, and the full name for the abbreviation of each vegetation type is provided in the caption of Fig. 1.

consequently no differences existed in the estimated annual GPP and ET.

Mean annual total GPP of China's terrestrial ecosystems over the period 2003–2012 was 6.32 Pg C yr^{-1}, 6.15 Pg C yr^{-1}, and 5.16 Pg C yr^{-1} for GLASS-GPP, FSGOM-GPP, and MCD15-GPP, respectively. GLASS-GPP and FSGOM-GPP were 22.5% and 19.2% higher than MCD15-GPP. The national annual mean ET based on the GLASS, FSGOM, and MCD15 LAI was 379.9 mm yr^{-1} (i.e., 3.58 × 10^3 km^3), 374.4 mm yr^{-1} (i.e., 3.53 × 10^3 km^3), 352.1 mm yr^{-1} (i.e., 3.32 × 10^3 km^3), respectively. GLASS-ET and FSGOM-ET were 7.9% and 6.3% higher than MCD15-ET, respectively.

3.5. Trends of simulated annual GPP and annual ET

We examined the trends of simulated annual GPP and annual ET during the period 2003–2012 (Fig. 11). Differences in the trends of different LAI products resulted in discrepancies of trends in simulated GPP and ET. Annual GPP generally increased in areas with increasing LAI and decreased in areas with decreasing LAI (Fig. 11a–c). GLASS-GPP and MCD15-GPP increased over 15.9% and 17.3% of China's vegetated area, respectively, and decreased over 9.4% and 9.3% of the vegetated areas, respectively. FSGOM LAI led to slightly lower percentage area with increasing GPP (12.6%) than GLASS and MCD15 LAI and similar percentage area with decreasing GPP (~8.7%).

For each LAI product, the trends in the resulting annual ET showed similar patterns as the trends in the resulting annual GPP (Fig. 11). The simulated ET generally increased in areas with increasing LAI and decreased in areas with decreasing LAI (Fig. 11d–f). GLASS-ET, MCD15-ET and FSGOM-ET exhibited decreasing trends in 9.9%, 9.3% and 9.1% of the vegetated area, respectively, and increased in 5.7%, 5.8%, and 3.9% of the vegetated area, respectively.

The trends of nationally-integrated annual GPP and nationally-averaged annual ET based on the three LAI products during the period 2003–2012 are shown in Fig. 12. The nationally-integrated GPP exhibited insignificant upward trends for all the LAI products (Fig. 12a). All the three LAI products led to decreasing trends in nationally-averaged annual ET in China's landmass, and these trends were statistically insignificant (Fig. 12b). The insignificantly decreasing trend in FSGOM and increasing trends in GLASS and MCD15 (Fig. 4d) altered the magnitude but not the direction of the trends in nationally-integrated GPP and nationally-averaged annual ET.

4. Discussion

We examined the spatial consistency, long-term trends and accuracy of three satellite-derived LAI products (GLASS, MCD15, and FSGOM) for China at the decadal scale (2003 – 2012). Several previous studies also compared multiple LAI products. For example, Camacho et al. (2013) found discrepancies in the spatial and seasonal patterns in LAI among GEOV1, MODIS, CYCLOPES, and GLOBCARBON globally for the period 2003–2005 with the largest discrepancies for evergreen broadleaf forest and needleleaf forest. Fang et al. (2013a) found notable discrepancies in the spatial distribution and magnitude of LAI among MODIS, GEOV1, GLASS, GLOBMAP, and JRC-TIP products from 2003 to 2010. Our results showed that GLASS, MCD15, and FSGOM exhibited significant differences in magnitude and spatial patterns. These studies indicated that different LAI products exhibited large discrepancies in the magnitude and spatial patterns of LAI. LAI products could also differ in long-term trends in LAI. Although our results showed much smaller percentage land areas exhibiting increase in annual averaged LAI over the period 2003–2012 than a previous study based on LAI over the growing season (Piao et al., 2015), the percentage land area varied among the three LAI products.

Satellite-derived LAI products have been evaluated with finer-resolution LAI maps or field measurements (Camacho et al., 2013; Xiao et al., 2014). There is scale mismatch between the satellite-derived LAI products and field measurements, and the upscaling of LAI using finer-resolution imagery can bridge the gap between the LAI products and field LAI. However, there is significant uncertainty associated with upscaling, particularly in heterogeneous regions (Liu et al., 2012a). The discrepancies observed between the three LAI products and Landsat-based LAI maps could be attributed to the uncertainty in both LAI products and Landsat-based maps. The accuracy of LAI products has also been evaluated directly using field measurements, which involves scale mismatch but minimizes the uncertainty of the reference LAI data. Field LAI measurements were typically only made during a very limited number of specific dates. The collection of ground-based LAI time series will help evaluate the seasonality of the satellite-derived LAI products. The evaluation of multiple LAI products using finer-resolution or field LAI data can reveal the accuracy of each product to some extent. For example, Fang et al. (2012b) and Camacho et al. (2013) reported moderately high accuracy for the MODIS LAI product. A recent intercomparison study indicated improved quality of GLASS over MODIS LAI (Xiao et al., 2014). In mountainous areas in southwestern China, the performance of GLASS LAI was similar to or even slightly lower than MODIS LAI (Jin et al., 2017). Previous studies showed that LAI inverted using four-scale geometric optical model based algorithm had better quality than a previous version of the MODIS LAI product (Garrigues et al., 2008; Pisek et al., 2007). Our results showed that GLASS was slightly better than FSGOM and MCD15 in forest plots and FSGOM was slightly better than MCD15 and GLASS in grassland plots. These studies indicated that the accuracy assessment of LAI products depends on the quality of finer-resolution LAI data or the region of

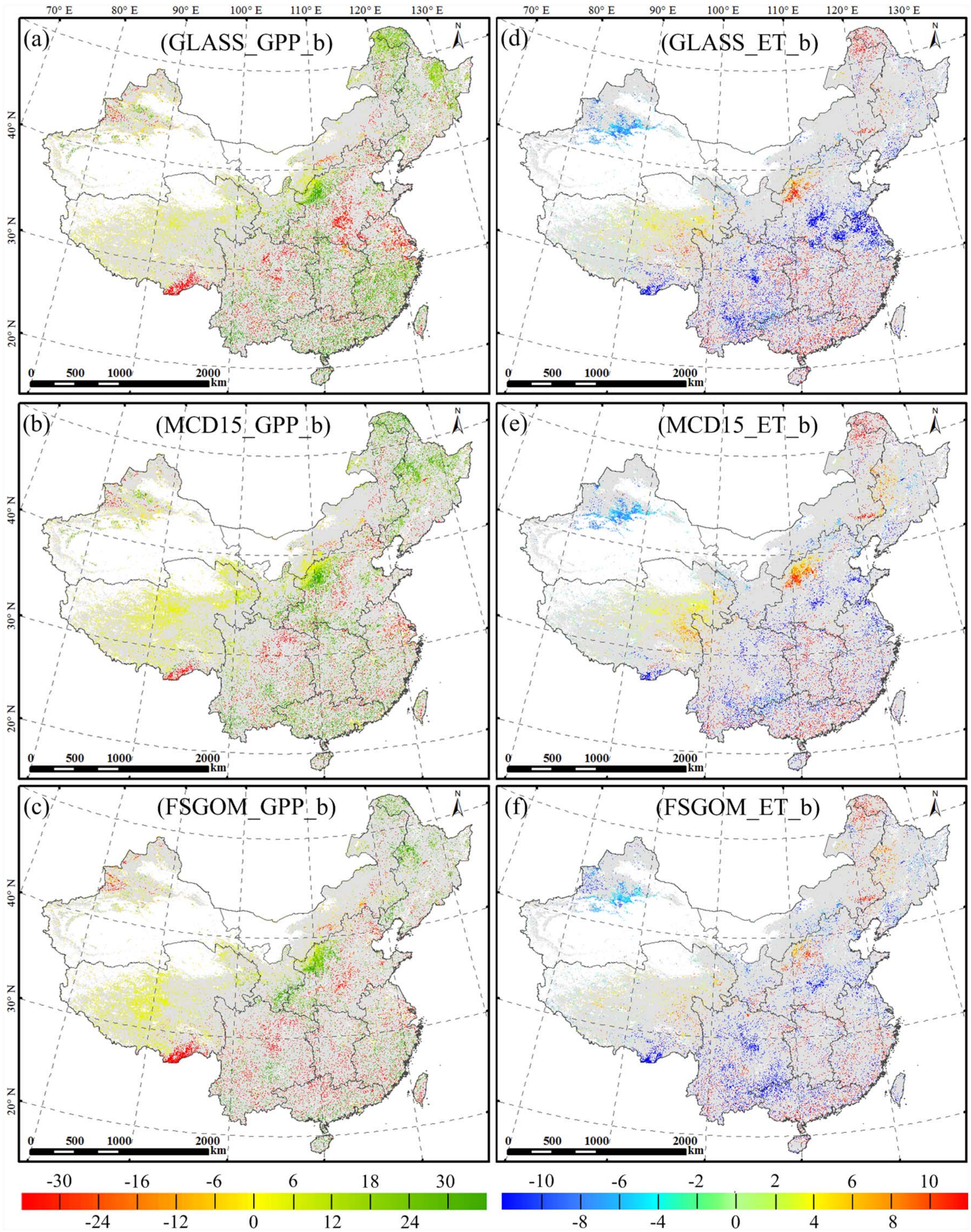

Fig. 11. Trends of annual GPP (g C m^{-2} yr^{-1}) and annual ET (mm yr^{-1}) during the period of 2003–2012: (a), (b), and (c) are GLASS-GPP, MCD15-GPP, and FSGOM-GPP, respectively; (d), (e), and (f) are GLASS-ET, MCD15-ET, and FSGOM-ET, respectively. The light gray indicates vegetated areas with insignificant trends in annual GPP or ET ($p > 0.05$).

interest.

The satellite-derived LAI products have different sources of uncertainty: input surface reflectance, retrieval algorithm, and the treatment of vegetation types (Fang et al., 2012a; Fang et al., 2013b). The discrepancies among the three LAI products could be largely attributed to the differences in the retrieval algorithms and the treatment of vegetation types. Although the three products were all based on MODIS reflectance for the period 2003–2012, they used different retrieval algorithms. The main algorithm of MCD15 employs biome-specific look-up tables simulated from three-dimensional radiative transfer model for retrieving LAI, while its backup algorithm is based on relationships between LAI and NDVI. FSGOM relies on land cover-specific relationships between LAI and a combination of red, near-infrared, and shortwave infrared bands reflectances simulated from the four-scale geometrical optical model (Chen and Leblanc, 1997). GLASS establishes the relationships between the fused LAI dataset from MODIS and CYCLOPES LAI products using biome-specific general regression neural networks (GRNN). Vegetation type is also an important source of uncertainty for different LAI products. The misclassification of vegetation type (or land cover) caused 15%–50% differences for LAI retrieval

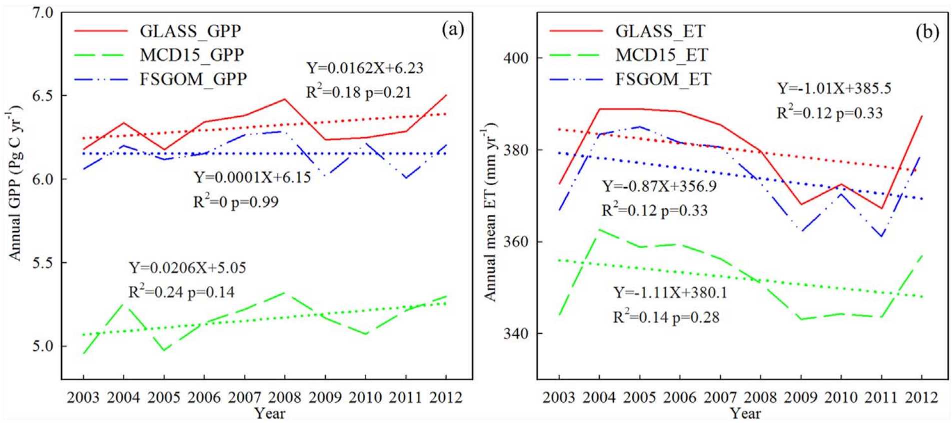

Fig. 12. Trends in nationally-integrated annual GPP (a) and nationally-averaged annual ET (b) based on the three LAI products during the period 2003–2012.

(Fang and Liang, 2005; Gonsamo and Chen, 2011) and unreasonable vegetation characterization induced 20% errors for the MODIS LAI product (Myneni et al., 2002). GLASS and MCD15 used slightly different vegetation types from FSGOM. Land cover misclassification or the use of different land cover datasets resulted in large discrepancies in retrieved LAI (Fang et al., 2013b; Liu et al., 2007). The availability of high quality and consistent surface reflectance and land cover data and sound retrieval algorithms will improve the accuracy of moderate resolution LAI products.

The comparison and evaluation of multiple LAI products can also help assess how the use of these products influences simulated GPP and ET. Several previous studies conducted site-level sensitivity analyses and showed that simulated GPP and ET were sensitive to LAI (Heinsch et al., 2006; Ryu et al., 2011). Unlike these studies, our study examined the effects of gridded LAI on simulated carbon and water fluxes at the national scale. Our results showed that the discrepancies in satellite-derived LAI products led to significant differences in the magnitude of annual GPP and ET at the national scale. These discrepancies could translate to larger differences in simulation of net carbon uptake and water yield. Accurate quantification of carbon uptake and ecosystem productivity (Xiao et al., 2015; Zhang et al., 2012c) and water balance (Hao et al., 2015) has important implications for climate policymaking. The discrepancies in LAI among the three LAI products also led to differences in the spatial patterns and trends of annual GPP and ET simulated by diagnostic ecosystem models. Having LAI products with reasonable spatial patterns and trends is essential for realistically simulating the patterns and trends of carbon and water fluxes and better informing climate policymaking.

Model simulations have three main sources of uncertainty: model input, model structure, and model parameters (Beck, 1987). Our study showed that besides meteorological data (Zhao et al., 2006) and land cover map (Xiao et al., 2011), the LAI products can also lead to significant uncertainty in simulated carbon and water fluxes, demonstrating that LAI is also an important source of uncertainty to the simulations of diagnostic ecosystem models (or terrestrial biosphere models). Further research is needed to disentangle the relative effects of LAI and other model input (e.g., meteorological data, land cover) on carbon and water cycle modeling. The discrepancies in LAI among the three LAI products also led to differences in the spatial patterns and trends of simulated annual GPP and ET. This indicates that the uncertainty in satellite LAI products can alter the spatial patterns and trends of carbon and water fluxes simulated by diagnostic ecosystem models. Developing more accurate LAI products will presumably reduce the uncertainty in simulated carbon and water fluxes.

Clumping index is an important parameter for accurate separation of sunlit and shaded leaf groups and accurate modeling of canopy-level vegetation photosynthesis and ET in terrestrial biosphere models (Chen et al., 2012; Ryu et al., 2011). Some previous studies demonstrated that ignoring clumping could significantly underestimate annual GPP (Chen et al., 2012) and ET (Chen et al., 2016) at broad and site scales, respectively. The three LAI products in this study adopted different clumping index accounting schemes. MODIS LAI takes clumping index at shoot and canopy scales into account and usually represents true LAI (Myneni et al., 2002), while GLASS and FSGOM both used vegetation type-dependent clumping index to produce true LAI from effective LAI. The use of different clumping index values for these products could lead to discrepancies among these products. The clumping index varies spatially and temporally, and the treatment of the index as constant for each specific vegetation type could also lead to overestimation or underestimation of LAI. Recently, a growing numbers of regional- and global-scale clumping index maps with increasing spatial resolution have been derived from satellite data (e.g., POLDER, MODIS, and MISR) (He et al., 2012; Pisek et al., 2013). Further incorporation of these gridded clumping index maps in prognostic terrestrial biosphere models will potentially lead to better characterization of plant canopies and hence better land-atmosphere interactions.

LAI was prescribed in our diagnostic terrestrial biosphere model, and the discrepancies in the satellite-derived LAI products led to significant uncertainty in the resulting GPP and ET estimates. Although prognostic models simulate LAI internally and do not require the prescribing of LAI, satellite-derived LAI products have been assimilated into prognostic terrestrial biosphere models for improved model estimates (Demarty et al., 2007; Kala et al., 2014). The assimilation of satellite-derived LAI products into prognostic models will presumably lead to significant uncertainty in the simulated carbon and water fluxes. The development of more accurate LAI products and their assimilation into model simulations will improve the simulation of carbon and water fluxes for terrestrial biosphere models.

5. Conclusions

In this study, the accuracy of three satellite-derived LAI products (GLASS, MCD15, and FSGOM) were firstly evaluated using fine-resolution gridded LAI derived from field plot measurements and Landsat imagery and annual maximum LAI data from EC flux sites across China. Our results showed that GLASS exhibited better performance than FSGOM and MCD15 for forests, while FSGOM was better than MCD15 and GLASS for grasslands. Systematic underestimation was observed for GLASS and MCD15 when the annual maximum LAI was > 3.0. The three LAI products differed in magnitude, spatial patterns, and trends in LAI. The three LAI products led to large differences in simulated annual GPP and ET at the regional scale. Mean annual total GPP for China's terrestrial ecosystems based on GLASS and FSGOM were 22.5% and 19.2% higher than that based on MCD15, respectively. During the period of 2003–2012, annual GPP simulated from GLASS and MCD15 increased over 15.9% and 17.3% of China's vegetated area while decreased over 9.4% and 9.3% of the vegetated area. FSGOM led to slightly lower percentage area with increasing GPP (12.6%) than GLASS

and MCD15 and similar percentage area with decreasing GPP (8.7%). National annual mean ET based on GLASS and FSGOM were 7.9% and 6.3% higher than that based on MCD15, respectively. Annual ET exhibited larger percentage areas with increasing ET trends for GLASS (5.7%) and MCD15 (5.8%) than for FSGOM (3.9%). Our study showed that the discrepancies in LAI can lead to substantial uncertainty in simulated carbon and water fluxes. The improvement of the satellite-derived LAI products will presumably improve regional- and global-scale carbon and water simulations of terrestrial biosphere models.

Acknowledgments

This research is supported by China's funding agencies (the National Key R&D Program of China: 2016YFA0600202; National Natural Science Foundation of China: 41401218, 41701393, 41271354; China Special Fund for Meteorological Research in the Public Interest: GYHY201506001-6) and U.S. funding agencies (National Aeronautics and Space Administration (NASA) through the Climate Indicators and Data Products for Future National Climate Assessments: NNX16AG61G and the Science of Terra and Aqua: NNX14AI70G; National Science Foundation (NSF) through MacroSystems Biology: EF-1065777, EF-1638688). We thank the three anonymous reviewers for their constructive and insightful comments on the manuscript.

Appendix A. Supplementary data

Supplementary data to this article can be found online at https://doi.org/10.1016/j.rse.2017.12.024.

References

Baker, I.T., Prihodko, L., Denning, A.S., Goulden, M., Miller, S., da Rocha, H.R., 2008. Seasonal drought stress in the Amazon: reconciling models and observations. J. Geophys. Res. Biogeosci. 113.

Baret, F., Hagolle, O., Geiger, B., Bicheron, P., Miras, B., Huc, M., Berthelot, B., Nino, F., Weiss, M., Samain, O., Roujean, J.L., Leroy, M., 2007. LAI, fAPAR and fCover CYCLOPES global products derived from VEGETATION - part 1: principles of the algorithm. Remote Sens. Environ. 110, 275–286.

Beck, M.B., 1987. Water quality modeling: a review of the analysis of uncertainty. Water Resour. Res. 23, 1393–1442.

Camacho, F., Cernicharo, J., Lacaze, R., Baret, F., Weiss, M., 2013. GEOV1: LAI, FAPAR essential climate variables and FCOVER global time series capitalizing over existing products. Part 2: validation and intercomparison with reference products. Remote Sens. Environ. 137, 310–329.

Chen, J.M., Black, T.A., 1992. Defining leaf-area index for non-flat leaves. Plant Cell Environ. 15, 421–429.

Chen, J.M., Leblanc, S.G., 1997. A four-scale bidirectional reflectance model based on canopy architecture. IEEE Trans. Geosci. Remote Sens. 35, 1316–1337.

Chen, J.M., Liu, J., Cihlar, J., Goulden, M.L., 1999. Daily canopy photosynthesis model through temporal and spatial scaling for remote sensing applications. Ecol. Model. 124, 99–119.

Chen, J.M., Mo, G., Pisek, J., Liu, J., Deng, F., Ishizawa, M., Chan, D., 2012. Effects of foliage clumping on the estimation of global terrestrial gross primary productivity. Glob. Biogeochem. Cycles 26, GB1019.

Chen, B., Liu, J., Chen, J.M., Croft, H., Gonsamo, A., He, L., Luo, X., 2016. Assessment of foliage clumping effects on evapotranspiration estimates in forested ecosystems. Agric. For. Meteorol. 216, 82–92.

Cohen, W.B., Maiersperger, T.K., Yang, Z.Q., Gower, S.T., Turner, D.P., Ritts, W.D., Berterretche, M., Running, S.W., 2003. Comparisons of land cover and LAI estimates derived from ETM plus and MODIS for four sites in North America: a quality assessment of 2000/2001 provisional MODIS products. Remote Sens. Environ. 88, 233–255.

Demarty, J., Chevallier, F., Friend, A.D., Viovy, N., Piao, S., Ciais, P., 2007. Assimilation of global MODIS leaf area index retrievals within a terrestrial biosphere model. Geophys. Res. Lett. 34, L15402.

Deng, F., Chen, J.M., Plummer, S., Chen, M.Z., Pisek, J., 2006. Algorithm for global leaf area index retrieval using satellite imagery. IEEE Trans. Geosci. Remote Sens. 44, 2219–2229.

Fang, H.L., Liang, S.L., 2005. A hybrid inversion method for mapping leaf area index from MODIS data: experiments and application to broadleaf and needleleaf canopies. Remote Sens. Environ. 94, 405–424.

Fang, H., Wei, S., Jiang, C., Scipal, K., 2012a. Theoretical uncertainty analysis of global MODIS, CYCLOPES, and GLOBCARBON LAI products using a triple collocation method. Remote Sens. Environ. 124, 610–621.

Fang, H.L., Wei, S.S., Liang, S.L., 2012b. Validation of MODIS and CYCLOPES LAI products using global field measurement data. Remote Sens. Environ. 119, 43–54.

Fang, H., Jiang, C., Li, W., Wei, S., Baret, F., Chen, J.M., Garcia-Haro, J., Liang, S., Liu, R., Myneni, R.B., Pinty, B., Xiao, Z., Zhu, Z., 2013a. Characterization and intercomparison of global moderate resolution leaf area index (LAI) products: analysis of climatologies and theoretical uncertainties. J. Geophys. Res. Biogeosci. 118, 529–548.

Fang, H.L., Li, W.J., Myneni, R.B., 2013b. The impact of potential land cover misclassification on MODIS leaf area index (LAI) estimation: a statistical perspective. Remote Sens. 5, 830–844.

Fang, Y., Sun, G., Caldwell, P., McNulty, S.G., Noormets, A., Domec, J.-C., King, J., Zhang, Z., Zhang, X., Lin, G., Zhou, G., Xiao, J., Chen, J., 2016. Monthly land cover-specific evapotranspiration models derived from global eddy flux measurements and remote sensing data. Ecohydrology 9, 248–266.

Feng, X., Liu, G., Chen, J.M., Chen, M., Liu, J., Ju, W.M., Sun, R., Zhou, W., 2007. Net primary productivity of China's terrestrial ecosystems from a process model driven by remote sensing. J. Environ. Manag. 85, 563–573.

Friedl, M.A., Sulla-Menashe, D., Tan, B., Schneider, A., Ramankutty, N., Sibley, A., Huang, X.M., 2010. MODIS collection 5 global land cover: algorithm refinements and characterization of new datasets. Remote Sens. Environ. 114, 168–182.

Garrigues, S., Lacaze, R., Baret, F., Morisette, J.T., Weiss, M., Nickeson, J.E., Fernandes, R., Plummer, S., Shabanov, N.V., Myneni, R.B., Knyazikhin, Y., Yang, W., 2008. Validation and intercomparison of global leaf area index products derived from remote sensing data. J. Geophys. Res. Biogeosci. 113, G02028.

Gonsamo, A., Chen, J.M., 2011. Evaluation of the GLC2000 and NALC2005 land cover products for LAI retrieval over Canada. Can. J. Remote. Sens. 37, 302–313.

Gonsamo, A., Chen, J.M., 2014. Improved LAI algorithm implementation to MODIS data by incorporating background, topography, and foliage clumping information. IEEE Trans. Geosci. Remote Sens. 52, 1076–1088.

Hao, L., Sun, G., Liu, Y., Wan, J., Qin, M., Qian, H., Liu, C., Zheng, J., John, R., Fan, P., Chen, J., 2015. Urbanization dramatically altered the water balances of a paddy field-dominated basin in southern China. Hydrol. Earth Syst. Sci. 19, 3319–3331.

He, L., Chen, J.M., Pisek, J., Schaaf, C.B., Strahler, A.H., 2012. Global clumping index map derived from the MODIS BRDF product. Remote Sens. Environ. 119, 118–130.

Heinsch, F.A., Zhao, M.S., Running, S.W., Kimball, J.S., Nemani, R.R., Davis, K.J., Bolstad, P.V., Cook, B.D., Desai, A.R., Ricciuto, D.M., Law, B.E., Oechel, W.C., Kwon, H., Luo, H.Y., Wofsy, S.C., Dunn, A.L., Munger, J.W., Baldocchi, D.D., Xu, L.K., Hollinger, D.Y., Richardson, A.D., Stoy, P.C., Siqueira, M.B.S., Monson, R.K., Burns, S.P., Flanagan, L.B., 2006. Evaluation of remote sensing based terrestrial productivity from MODIS using regional tower eddy flux network observations. IEEE Trans. Geosci. Remote Sens. 44, 1908–1925.

IPCC, 2013. Climate Change 2013: The Physical Science Basis. Contribution of Working Group I to the Fifth Assessment Report of the Intergovernmental Panel on Climate Change. Cambridge University Press, Cambridge, United Kingdom and New York, NY, USA.

Jarvis, P.G., 1976. The interpretation of variations in leaf water potential and stomatal conductance found in canopies in field. Philos. Trans. R. Soc. Lond. Ser. B Biol. Sci. 273, 593–610.

Jiang, C., Ryu, Y., Fang, H., Myneni, R., Claverie, M., Zhu, Z., 2017. Inconsistencies of interannual variability and trends in long-term satellite leaf area index products. Glob. Chang. Biol. 23, 4133–4146.

Jin, H., Li, A., Bian, J., Nan, X., Zhao, W., Zhang, Z., Yin, G., 2017. Intercomparison and validation of MODIS and GLASS leaf area index (LAI) products over mountain areas: a case study in southwestern China. Int. J. Appl. Earth Obs. Geoinf. 55, 52–67.

Ju, W.M., Chen, J.M., Black, T.A., Barr, A.G., Liu, J., Chen, B.Z., 2006. Modelling multi-year coupled carbon and water fluxes in a boreal aspen forest. Agric. For. Meteorol. 140, 136–151.

Kala, J., Decker, M., Exbrayat, J.-F., Pitman, A.J., Carouge, C., Evans, J.P., Abramowitz, G., Mocko, D., 2014. Influence of leaf area index prescriptions on simulations of heat, moisture, and carbon fluxes. J. Hydrometeorol. 15, 489–503.

Keeling, C.D., Bacastow, R.B., Bainbridge, A.E., Ekdahl, C.A., Guenther, P.R., Waterman, L.S., Chin, J.F.S., 1976. Atmospheric carbon dioxide variations at Mauna Loa Observatory, Hawaii. Tellus 28, 538–551.

Li, D., Ju, W., Lu, D., Zhou, Y., Wang, H., 2015. Impact of estimated solar radiation on gross primary productivity simulation in subtropical plantation in southeast China. Sol. Energy 120, 175–186.

Liang, S.L., Zhao, X., Liu, S.H., Yuan, W.P., Cheng, X., Xiao, Z.Q., Zhang, X.T., Liu, Q., Cheng, J., Tang, H.R., Qu, Y.H., Bo, Y.C., Qu, Y., Ren, H.Z., Yu, K., Townshend, J., 2013. A long-term Global LAnd Surface Satellite (GLASS) data-set for environmental studies. Int. J. Digital Earth 6, 5–33.

Liu, J., Chen, J.M., Cihlar, J., Park, W.M., 1997. A process-based boreal ecosystem productivity simulator using remote sensing inputs. Remote Sens. Environ. 62, 158–175.

Liu, J., Chen, J.M., Cihlar, J., 2003. Mapping evapotranspiration based on remote sensing: an application to Canada's landmass. Water Resour. Res. 39, 1189.

Liu, R., Chen, J.M., Liu, J., Deng, F., Sun, R., 2007. Application of a new leaf area index algorithm to China's landmass using MODIS data for carbon cycle research. J. Environ. Manag. 85, 649–658.

Liu, Y., Ju, W., Zhu, G., Chen, J., Xing, B., Zhu, J., Zhou, Y., 2011. Retrieval of leaf area index for different grasslands in Inner Mongolia prairie using remote sensing data. Acta Ecol. Sin. 31, 5159–5170.

Liu, Y., Ju, W., Chen, J., Zhu, G., Xing, B., Zhu, J., He, M., 2012a. Spatial and temporal variations of forest LAI in China during 2000–2010. Chin. Sci. Bull. 57, 2846–2856.

Liu, Y., Liu, R., Chen, J.M., 2012b. Retrospective retrieval of long-term consistent global leaf area index (1981–2011) from combined AVHRR and MODIS data. J. Geophys. Res. Biogeosci. 117, G04003.

Liu, Y., Ju, W., He, H., Wang, S., Sun, R., Zhang, Y., 2013a. Changes of net primary productivity in China during recent 11 years detected using an ecological model driven by MODIS data. Front. Earth Sci. 7, 112–127.

Liu, Y., Zhou, Y., Ju, W., Chen, J., Wang, S., He, H., Wang, H., Guan, D., Zhao, F., Li, Y., Hao, Y., 2013b. Evapotranspiration and water yield over China's landmass from 2000 to 2010. Hydrol. Earth Syst. Sci. 17, 4957–4980.

Liu, Z., Shao, Q., Liu, J., 2014. The performances of MODIS-GPP and -ET products in China and their sensitivity to input data (FPAR/LAI). Remote Sens. 7, 135–152.

Liu, Y., Xiao, J., Ju, W., Zhou, Y., Wang, S., Wu, X., 2015. Water use efficiency of China's terrestrial ecosystems and responses to drought. Sci. Rep. 5, 13799. http://dx.doi.org/10.1038/srep13799.

Liu, Y., Xiao, J., Ju, W., Xu, K., Zhou, Y., Zhao, Y., 2016. Recent trends in vegetation greenness in China significantly altered annual evapotranspiration and water yield. Environ. Res. Lett. 11, 094010. http://dx.doi.org/10.1088/1748-9326/11/9/094010.

Morisette, J.T., Baret, F., Privette, J.L., Myneni, R.B., Nickeson, J.E., Garrigues, S., Shabanov, N.V., Weiss, M., Fernandes, R.A., Leblanc, S.G., Kalacska, M., Sanchez-Azofeifa, G.A., Chubey, M., Rivard, B., Stenberg, P., Rautiainen, M., Voipio, P., Manninen, T., Pilant, A.N., Lewis, T.E., Iiames, J.S., Colombo, R., Meroni, M., Busetto, L., Cohen, W.B., Turner, D.P., Warner, E.D., Petersen, G.W., Seufert, G., Cook, R., 2006. Validation of global moderate-resolution LAI products: a framework proposed within the CEOS Land Product Validation subgroup. IEEE Trans. Geosci. Remote Sens. 44, 1804–1817.

Mu, Q., Heinsch, F.A., Zhao, M., Running, S.W., 2007. Development of a global evapotranspiration algorithm based on MODIS and global meteorology data. Remote Sens. Environ. 111, 519–536.

Myneni, R.B., Hoffman, S., Knyazikhin, Y., Privette, J.L., Glassy, J., Tian, Y., Wang, Y., Song, X., Zhang, Y., Smith, G.R., Lotsch, A., Friedl, M., Morisette, J.T., Votava, P., Nemani, R.R., Running, S.W., 2002. Global products of vegetation leaf area and fraction absorbed PAR from year one of MODIS data. Remote Sens. Environ. 83, 214–231.

Oleson, K., Lawrence, D.M., Bonan, G.B., Drewniak, B., Huang, M., Koven, C.D., Levis, S., Li, F., Riley, W.J., Subin, Z.M., Swenson, S., Thornton, P.E., Bozbiyik, A., Fisher, R., Heald, C.L., Kluzek, E., Lamarque, J.-F., Lawrence, P.J., Leung, L.R., Lipscomb, W., Muszala, S.P., Ricciuto, D.M., Sacks, W.J., Sun, Y., Tang, J., Yang, Z.-L., 2013. Technical description of version 4.5 of the Community Land Model (CLM). In: NCAR Technical Note NCAR/TN-503 + STR. National Center for Atmospheric Research, Boulder, Colorado.

Piao, S., Yin, G., Tan, J., Cheng, L., Huang, M., Li, Y., Liu, R., Mao, J., Myneni, R.B., Peng, S., Poulter, B., Shi, X., Xiao, Z., Zeng, N., Zeng, Z., Wang, Y., 2015. Detection and attribution of vegetation greening trend in China over the last 30 years. Glob. Chang. Biol. 21, 1601–1609.

Pisek, J., Chen, J.M., Deng, F., 2007. Assessment of a global leaf area index product from SPOT-4 VEGETATION data over selected sites in Canada. Can. J. Remote. Sens. 33, 341–356.

Pisek, J., Chen, J.M., Lacaze, R., Sonnentag, O., Alikas, K., 2010. Expanding global mapping of the foliage clumping index with multi-angular POLDER three measurements: evaluation and topographic compensation. ISPRS J. Photogramm. Remote Sens. 65, 341–346.

Pisek, J., Ryu, Y., Sprintsin, M., He, L., Oliphant, A.J., Korhonen, L., Kuusk, J., Kuusk, A., Bergstrom, R., Verrelst, J., Alikas, K., 2013. Retrieving vegetation clumping index from Multi-angle Imaging SpectroRadiometer (MISR) data at 275 m resolution. Remote Sens. Environ. 138, 126–133.

Running, S.W., Nemani, R.R., Heinsch, F.A., Zhao, M.S., Reeves, M., Hashimoto, H., 2004. A continuous satellite-derived measure of global terrestrial primary production. Bioscience 54, 547–560.

Ryu, Y., Baldocchi, D.D., Kobayashi, H., van Ingen, C., Li, J., Black, T.A., Beringer, J., van Gorsel, E., Knohl, A., Law, B.E., Roupsard, O., 2011. Integration of MODIS land and atmosphere products with a coupled-process model to estimate gross primary productivity and evapotranspiration from 1 km to global scales. Glob. Biogeochem. Cycles 25, GB4017.

Sawada, Y., Koike, T., 2014. Simultaneous estimation of both hydrological and ecological parameters in an ecohydrological model by assimilating microwave signal. J. Geophys. Res. Atmos. 119, 8839–8857.

Schaefer, K., Schwalm, C.R., Williams, C., Arain, M.A., Barr, A., Chen, J.M., Davis, K.J., Dimitrov, D., Hilton, T.W., Hollinger, D.Y., Humphreys, E., Poulter, B., Raczka, B.M., Richardson, A.D., Sahoo, A., Thornton, P., Vargas, R., Verbeeck, H., Anderson, R., Baker, I., Black, T.A., Bolstad, P., Chen, J., Curtis, P.S., Desai, A.R., Dietze, M., Dragoni, D., Gough, C., Grant, R.F., Gu, L., Jain, A., Kucharik, C., Law, B., Liu, S., Lokipitiya, E., Margolis, H.A., Matamala, R., McCaughey, J.H., Monson, R., Munger, J.W., Oechel, W., Peng, C., Price, D.T., Ricciuto, D., Riley, W.J., Roulet, N., Tian, H., Tonitto, C., Torn, M., Weng, E., Zhou, X., 2012. A model-data comparison of gross primary productivity: results from the North American Carbon Program site synthesis. J. Geophys. Res. Biogeosci. 117, G03010.

Shangguan, W., Dai, Y., Liu, B., Ye, A., Yuan, H., 2012. A soil particle-size distribution dataset for regional land and climate modelling in China. Geoderma 171-172, 85–91.

Tang, S., Chen, J.M., Zhu, Q., Li, X., Chen, M., Sun, R., Zhou, Y., Deng, F., Xie, D., 2007. LAI inversion algorithm based on directional reflectance kernels. J. Environ. Manag. 85, 638–648.

Taylor, K.E., 2001. Summarizing multiple aspects of model performance in a single diagram. J. Geophys. Res.-Atmos. 106, 7183–7192.

Thorn, A.M., Xiao, J., Ollinger, S.V., 2015. Generalization and evaluation of the process-based forest ecosystem model PnET-CN for other biomes. Ecosphere 6, 43. http://dx.doi.org/10.1890/ES14-00542.1.

Xiao, Z.Q., 2013. Global LAnd Surface Satellite (GLASS) LAI product. In: Symposium on Retrieval Theories and Methods of Land Surface Satellite Remote Sensing Data, July 15, 2013, Beijing, China.

Xiao, J.F., Zhuang, Q.L., Liang, E.Y., McGuire, A.D., Moody, A., Kicklighter, D.W., Shao, X.M., Melillo, J.M., 2009. Twentieth-century droughts and their impacts on terrestrial carbon cycling in China. Earth Interact. 13, 10. http://dx.doi.org/10.1175/2009EI275.1.

Xiao, J.F., Davis, K.J., Urban, N.M., Keller, K., Saliendra, N.Z., 2011. Upscaling carbon fluxes from towers to the regional scale: influence of parameter variability and land cover representation on regional flux estimates. J. Geophys. Res. 116, G00J06. http://dx.doi.org/10.1029/2010JG001568.

Xiao, Z.Q., Liang, S.L., Wang, J.D., Chen, P., Yin, X.J., Zhang, L.Q., Song, J.L., 2014. Use of general regression neural networks for generating the GLASS leaf area index product from time-series MODIS surface reflectance. IEEE Trans. Geosci. Remote Sens. 52, 209–223.

Xiao, J.F., Zhou, Y., Zhang, L., 2015. Contributions of natural and human factors to increases in vegetation productivity in China. Ecosphere 6, 233. http://dx.doi.org/10.1890/ES14-00394.1.

Yan, M., Tian, X., Li, Z., Chen, E., Li, C., Fan, W., 2016. A long-term simulation of forest carbon fluxes over the Qilian Mountains. Int. J. Appl. Earth Obs. Geoinf. 52, 515–526.

Yang, W., Shabanov, N.V., Huang, D., Wang, W., Dickinson, R.E., Nemani, R.R., Knyazikhin, Y., Myneni, R.B., 2006. Analysis of leaf area index products from combination of MODIS Terra and Aqua data. Remote Sens. Environ. 104, 297–312.

Zhang, F., Chen, J.M., Chen, J., Gough, C.M., Martin, T.A., Dragoni, D., 2012a. Evaluating spatial and temporal patterns of MODIS GPP over the conterminous U.S. against flux measurements and a process model. Remote Sens. Environ. 124, 717–729.

Zhang, F., Ju, W., Shen, S., Wang, S., Yu, G., Han, S., 2012b. Variations of terrestrial net primary productivity in East Asia. Terr. Atmos. Ocean. Sci. 23, 425–437.

Zhang, F.M., Chen, J.M., Pan, Y.D., Birdsey, R.A., Shen, S.H., Ju, W.M., He, L.M., 2012c. Attributing carbon changes in conterminous U.S. forests to disturbance and non-disturbance factors from 1901 to 2010. J. Geophys. Res. Biogeosci. 117, G02021. http://dx.doi.org/10.1029/2011JG001930.

Zhao, M., Running, S.W., Nemani, R.R., 2006. Sensitivity of Moderate Resolution Imaging Spectroradiometer (MODIS) terrestrial primary production to the accuracy of meteorological reanalyses. J. Geophys. Res. Biogeosci. 111, G01002.

Zhu, Z., Bi, J., Pan, Y., Ganguly, S., Anav, A., Xu, L., Samanta, A., Piao, S., Nemani, R., Myneni, R., 2013. Global data sets of vegetation leaf area index (LAI)3g and fraction of photosynthetically active radiation (FPAR)3g derived from global inventory modeling and mapping studies (GIMMS) normalized difference vegetation index (NDVI3g) for the period 1981 to 2011. Remote Sens. 5, 927–948.

Zhu, H., Lin, A., Wang, L., Xia, Y., Zou, L., 2016. Evaluation of MODIS gross primary production across multiple biomes in China using Eddy covariance flux data. Remote Sens. 8, 395.